Front. Chem. Sci. Eng. 2022, 16(6): 777−798
https://doi.org/10.1007/s11705-022-2148-0

REVIEW ARTICLE

Rational design on photoelectrodes and devices to boost photoelectrochemical performance of solar-driven water splitting: a mini review

Siliu Lyu[1*], Muhammad Adnan Younis[1*], Zhibin Liu (✉)[2], Libin Zeng[2], Xianyun Peng[2], Bin Yang[1], Zhongjian Li[1], Lecheng Lei[1,2], Yang Hou (✉)[1,2]

1 Key Laboratory of Biomass Chemical Engineering of Ministry of Education, College of Chemical and Biological Engineering, Zhejiang University, Hangzhou 310027, China
2 Institute of Zhejiang University-Quzhou, Quzhou 324000, China

Abstract As an eco-friendly, efficient, and low-cost technique, photoelectrochemical water splitting has attracted growing interest in the production of clean and sustainable hydrogen by the conversion of abundant solar energy. In the photoelectrochemical system, the photoelectrode plays a vital role in absorbing the energy of sunlight to trigger the water splitting process and the overall efficiency depends largely on the integration and design of photoelectrochemical devices. In recent years, the optimization of photoelectrodes and photoelectrochemical devices to achieve highly efficient hydrogen production has been extensively investigated. In this paper, a concise review of recent advances in the modification of nanostructured photoelectrodes and the design of photoelectrochemical devices is presented. Meanwhile, the general principles of structural and morphological factors in altering the photoelectrochemical performance of photoelectrodes are discussed. Furthermore, the performance indicators and first principles to describe the behaviors of charge carriers are analyzed, which will be of profound guiding significance to increasing the overall efficiency of the photoelectrochemical water splitting system. Finally, current challenges and prospects for an in-depth understanding of reaction mechanisms using advanced characterization technologies and potential strategies for developing novel photoelectrodes and advanced photoelectrochemical water splitting devices are demonstrated.

Keywords photoelectrochemical water splitting, photoelectrodes, hydrogen production, charge separation, catalytic mechanism

Received September 17, 2021; accepted November 23, 2021

E-mails: zhibin.liu@rub.de (Liu Z.), yhou@zju.edu.cn (Hou Y.)

* These authors contributed equally to this work.

1 Introduction

With the growing energy demand, there is an urgent need to develop safe, clean, and renewable energy to replace the current energy dominated by fossil fuels [1,2]. Solar energy is the most abundant and freely available energy resource on earth whose utilization exerts no harmful impact on the natural ecosystem [3]. About 36000 TW solar energy reaches the land every year [4], only one-thousandth of which is sufficient to meet the global energy demand. Therefore, a great deal of work has been carried out to convert solar energy into applicable forms like electricity, thermal energy, chemical energy, and fuels [5−10]. Among these green energy sources, hydrogen has shown great potential to be an amazing renewable energy carrier [11−14], which could be directly applied to a combustion process to release heat without carbon dioxide emission or converted into other resources through fuel cells or classic chemical reactions (e.g., Fischer-Tropsch reaction and ammonia synthesis). Therefore, converting abundant solar energy into clean and renewable hydrogen could broaden its application scope and alleviate the energy crisis.

This conversion could be realized through photochemical and photoelectrochemical (PEC) systems where water is split into hydrogen [15−17]. In a photochemical water splitting system, photocatalysts are dispersed in water and generate hydrogen in the solution under visible light irradiation, which is easy to operate but has certain limitations like the low efficiency and mixed gaseous products of hydrogen and oxygen. In contrast, the PEC water splitting system uses photoelectrodes to separate products where hydrogen is produced at the cathode while oxygen is at the anode, as shown in Fig. 1. In the PEC water splitting system, an external bias could be

applied to improve its performance by accelerating the separation of photogenerated electrons and holes [18]. Thus, more attention has been paid to the efficient PEC water splitting system. This system consists of three steps, namely light-harvesting by photoelectrodes, the separation and transport of photogenerated charge carriers, and surface redox reactions [19,20]. All these procedures are vital to achieving the desired PEC water splitting performance, especially the photoelectrodes that are the core components intensively involved in them. In 1972, Fujishima and Honda reported a PEC water splitting system comprised of an *n*-type TiO_2 photoanode and a Pt cathode [21]. Since then, numerous efforts have been devoted to the reasonable design and optimization of photoelectrodes like compositions, structural and morphological control, and element doping, thus improving the active sites and electronic structures and overcoming the defects of photoelectrodes to facilitate the PEC water splitting process. Moreover, theoretical studies have been conducted on the excitation of photogenerated electron-hole pairs, the separation of the charge carriers, and their transport at the interfaces of photoelectrode/electrolyte for further redox reactions [22−24]. Research on these dynamic processes of charge carriers could provide a comprehensive understanding of their underlying mechanisms, thus further guiding the development of advanced photoelectrodes. Furthermore, device engineering is also essential to maximize the utilization efficiency and prolong the stability of each component in PEC devices in practical application. Generally, a PEC water splitting device consists of photoelectrodes, electrocatalysts, electrolytes, and membrane separators [25−27]. When the highly efficient and stable photoelectrodes are assembled into a PEC cell with a given geometry, the optimal performance might not be achieved due to the mismatches between different components [28−30]. Due to the limit of the operation conditions like the light absorption range [31], light intensity [32], pH of electrolyte [33], and operating temperature [34], the performance of photoelectrodes in the assembled cell might be inferior to the performance of those obtained in separate tests. Therefore, the selection of suitable photoelectrodes and construction of effective devices should be carefully coordinated to build high-performance devices, thus promoting the PEC water splitting technique to further realize the large-scale production of hydrogen.

This review covers the basic process that occurs in the PEC water splitting system, the performance evaluation parameters and theoretical investigation on behaviors of charge carriers, as well as the rational designs of the core photoelectrodes and devices. In addition, the optimization strategies for photoelectrodes construction are summarized, including crystallinity, size, bandgap, fabrication process, and other closely related factors. As for the device construction, four types of cell architectures are presented, i.e., single photoelectrode-based cell, Z-scheme, tandem, and monolithic PEC systems. Furthermore, the current challenges and prospects for the future development of the PEC water splitting technique are also demonstrated.

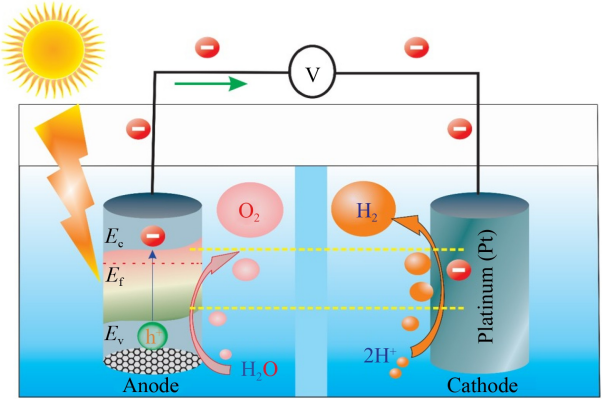

Fig. 1 Schematic of PEC water splitting by using a semiconductor material.

2 Basic mechanism involved in the PEC water splitting

The basic PEC water splitting mechanism involves multiple physiochemical processes [35]. When a solar photon is absorbed by semiconductors, a pair of electron-hole charge carriers will be formed in semiconductors. Afterward, these charge carriers are transferred and separated and the excited electrons are passed to conduct the hydrogen evolution reaction (HER) while the holes are consumed for the oxygen evolution reaction (OER) [36−39].

The reactions involved in the PEC water splitting are as follows [40]:

$$\mathrm{HER}: 4H^+ + 4e^-_{cb} \rightarrow 2H_2 \quad (1)$$

$$\mathrm{OER}: 2H_2O + 4h^+_{vb} \rightarrow O_2 + 4H^+ \quad (2)$$

$$\text{Overall reaction}: 2H_2O \rightarrow 2H_2 + O_2,\ \Delta G^o = 237\ \mathrm{kJ \cdot mol^{-1}} \quad (3)$$

where e^-_{cb} represents the photogenerated electrons in the conduction band (CB) while h^+_{vb} represents the photogenerated holes in the valence band (VB). According to the Planck-Einstein relation, photon energy of 1.23 eV is almost equal to the wavelength of 1008 nm [41], indicating that the photons present in the solar spectrum contain sufficient energy for splitting water. Theoretically, water has a transparent nature in the UV-visible range of 350−800 nm, whereas the sunlight at a wavelength lower than 190 nm could only accomplish the auto-photolysis of water. Moreover, it has been observed that when a semiconductor utilizes wavelengths of < 600 nm, its solar conversion efficiency will increase from 2% to 16%. Therefore, the PEC water splitting under visible light irradiation has received great attention since the 1970s [21,25,42,43].

The photoelectrode of the light absorption component is composed of *n*-type or *p*-type semiconductors acting as photoanodes and photocathodes, respectively [36]. When

a photon with greater energy than the bandgap energy (E_g) of photoelectrodes is absorbed, a pair of charge carriers will be created to excite electrons to the CB and leave holes in the VB. The potential of VB should be greater than the redox potential of O_2/H_2O, which is 1.23 V *vs.* NHE (normal hydrogen electrode) at pH = 0, to motivate the water oxidation (i.e., OER). Besides, the potential of CB should be more negative than the redox potential of H^+/H_2 (0 V *vs.* NHE at pH = 0) in order to carry out the reduction of water (i.e., HER) [37,39,44].

The transportation and separation processes of photogenerated electron-hole pairs are closely related to the band bending phenomenon that occurs at semiconductors. Once a semiconductor is immersed into an electrolyte solution, there will be an electron transfer process at the interface of the semiconductor and electrolyte to reach an equilibration state. In this state, the Fermi level of semiconductors is equilibrated with the oxidation-reduction potential of electrolyte solution. This electron transfer behavior at the interface causes a band bending of semiconductors, which is the driving force for the separation of electron-hole charge carriers [4,45]. A more detailed explanation of the separation and transport of charge carriers will be presented in section 5.

The last step comprises redox reactions, which occur at the surface of the catalyst to conduct water splitting. Both the appropriate reaction dynamics and charge carrier potential are critical for the high-efficiency PEC water splitting. Compared with the theoretical value of 1.23 V *vs.* reversible hydrogen electrode (RHE), the additional potential is required to drive the water splitting process, which is termed "overpotential". The overpotential compensates for the energy loss when holes pass through the space charge region and electrons move to the counter electrode via an external circuit [46]. Besides, the overpotential is also applied to overcome the energy barriers related to oxidation and reduction reactions.

3 Photoelectrodes for the PEC water splitting

The basic principles for photoelectrolysis energetics have been studied and explored for decades [38,47,48]. In terms of photoelectrocatalysis, there are two minimum requirements for a semiconductor photoelectrode to conduct water splitting without any applied voltages. First, the stored free energy during the photogeneration of electron-hole pairs should exceed 1.23 eV (at 298 K) to successfully conduct the energy separation between the O_2/H_2O and H^+/H_2 redox energy levels. Second, the free energy levels of the electrons and holes must straddle the redox energy levels of O_2/H_2O and H^+/H_2 to proceed with both water oxidation and proton reduction. Generally, an E_g significantly larger than 1.23 eV is required to overcome the overpotentials of these redox reactions [49,50]. The VB and CB positions of various semiconductors in correspondence with the reversible H_2 and O_2 redox energies at pH = 7 are shown in Fig. 2 [51]. Among the oxides shown in Fig. 2, only those with a wide bandgap (e.g., $SrTiO_3$) could conform to the above-listed principles. However, the solar-to-hydrogen (STH) efficiency of $SrTiO_3$ is rather low because it could only absorb the UV light of the solar spectrum [52]. Therefore, certain efforts have been made to focus on the integration of wide bandgap oxides with semiconductor materials to fabricate promising metal oxides-based photoelectrodes which could absorb a wide spectrum of solar light to split water into hydrogen and oxygen molecules. To this end, tandem systems are designed in which *n*-type and *p*-type semiconductors could be connected in an optical series to conduct PEC reactions [37,53]. Theoretically, if two photoelectrodes have considerable band gaps, the maximum efficiency of *n–p* tandem PEC devices can reach 46% and no additional energy will be required to conduct overall water splitting. However, the experimental efficiency could not reach the maximum theoretical efficiency. One of the main causes for this efficiency loss is the recombination of photogenerated electrons and holes. In a PEC cell, the recombination becomes acute. For example, in the photoanode, the water oxidation involved with four electrons is much slower than the reduction of protons by two electrons, resulting in mismatched consumptions of electrons and holes. Moreover, the reaction of holes generating O_2 also generates some intermediate species in the four-electron process when it occurs at the surface of an *n*-type photoanode, which ultimately traps electrons from CB. In both cases, recombination might occur and lead to low efficiency of the PEC water splitting [30,47,54]. Hence it is necessary to enhance the photoanode efficiency by increasing the interfacial electron transfer rate and decreasing the recombination rate.

In a tandem cell-based PEC device, a tandem configuration is designed in which a conventional solar cell is connected with photoelectrodes in an optical series to provide the additional bias needed to conduct the PEC water splitting [55]. This bias applied externally serves two purposes. First, it creates a depletion layer in the photoanode to facilitate the separation of photogenerated electron-hole pairs. Second, it facilitates the proton reduction by shifting the electrode potential of the metal-based cathode to a more negative direction compared with the reversible hydrogen potential. Therefore, the theoretical efficiency of this photovoltaic tandem arrangement is similar to that of an *n–p* tandem configuration [36,56,57].

4 Performance indicators for the PEC water splitting

After the fabrication of PEC devices, it is necessary to evaluate the parameters to determine their performance.

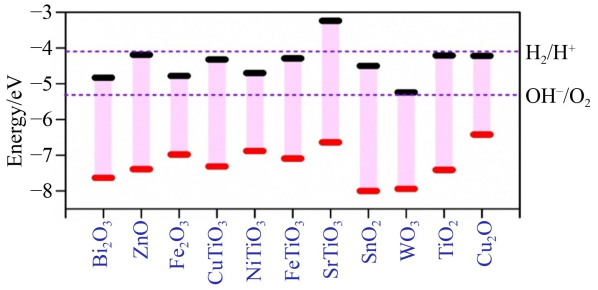

Fig. 2 The positions of VB and CB for several binary and ternary oxide semiconductors on the vacuum scale at pH = 7. The upper and lower dotted lines describe the energies of the reversible hydrogen and oxygen electrodes at pH = 7, respectively. Reprinted with permission from ref. [58], copyright 2014, Wiley-VCH.

As the ratio of the chemical energy stored in H_2 to the solar energy input, STH conversion efficiency defines the overall PEC performance of a device at solar Air Mass 1.5 Global (AM 1.5 G) illumination under zero bias conditions, set as a benchmark value to evaluate photoelectrode candidate materials in different electrolytes [36,59,60]. The STH could be calculated by the equation below [60]:

$$\mathrm{STH} = \left[\frac{|J_{sc}| \times 1.23\ (\mathrm{V}) \times \varnothing_F}{P}\right]_{\mathrm{AM\ 1.5\ G}} \times 100\%, \quad (4)$$

where J_{sc} is the short circuit photocurrent density of a PEC cell, $\varnothing_F$ denotes the Faradaic efficiency for hydrogen evolution, and P represents the power density of incident light.

The Faradaic efficiency of a PEC cell is calculated to evaluate the utilization of generated electrons, thus further probing the undesirable side reactions like photo corrosion. It could be calculated by the ratio of the evolved gas to the theoretically evolved gas about the measured photocurrent as below [61]:

$$\text{Faradaic efficiency } (H_2 \text{ or } O_2) = \frac{\text{Amount of } H_2 \text{ or } O_2 \text{ evolution}}{\text{Theoretical amount of } H_2 \text{ or } O_2 \text{ evolution}} \times 100\%. \quad (5)$$

Similarly, the parameter of incident photon-to-current efficiency (IPCE) could be employed to evaluate the quantum efficiency at a specific wavelength. It could be defined as the number of photogenerated charge carriers which contribute to the photocurrent per incident photon and calculated by the equation [4]:

$$\mathrm{IPCE}(\lambda) = \frac{\text{Total energy of converted electrons}}{\text{Total energy of incident photons}} = \frac{\left(\frac{J_{photo}(\lambda)}{e}\right) \times \left(\frac{hc}{\lambda}\right)}{P(\lambda)} \times 100\%, \quad (6)$$

where, h is the Planck constant, J_{photo} denotes the photocurrent density at the specific wavelength of the incident light, c represents the light speed, e is the charge of an electron, λ indicates the incident light wavelength, and $P(\lambda)$ denotes the incident light intensity at the particular wavelength.

In addition, other performance indicators like the applied bias photon-to-current efficiency and the absorbed photon-to-current conversion efficiency could also be applied to indicate the utilization of the absorbed sunlight.

5 Charge generation, transportation, and utilization

In general, some complicated PEC processes are usually involved in solar-driven water splitting, which are critical to the final PEC efficiency for water splitting. Therefore, the primary processes including charge generation, transportation, and utilization are presented in this section, as illustrated in Fig. 3. Meanwhile, the relevant contents of the first principles are also introduced to depict the energetic and dynamic behaviors of these three processes.

5.1 Charge generation

In the beginning, the energy of a photon is greater than the band gap of a semiconductor, an electron absorbs the photon and is excited from a filled VB to an empty CB, afterward a hole is generated in the VB and an electron is generated in the CB, resulting in an electron-hole pair. The holes are positively charged in an excited state while the electrons are negatively charged. In a semiconductor material, the VB band (occupied) and the CB band (unoccupied) are separated by a band gap, which could block the energy dissipation channels caused by the lack of accessible electronic states, thus efficiently preventing the energy from dissipation. When the absorbed photon energy is much larger than the band gap, the electrons might be transferred to higher states in the CB. This newly generated electron-hole pair is initially in a non-equilibrium state and afterward in an equilibrium state with extra energy exhausted due to the carrier–carrier interactions [22,38,47,62]. These interactions could be

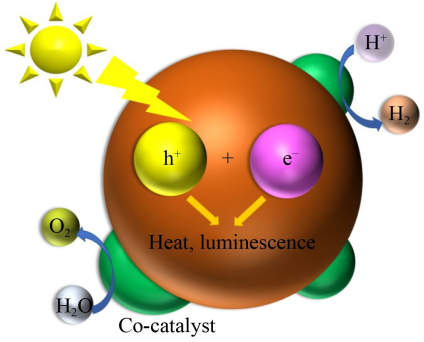

Fig. 3 Schematic processes of charge generation, transportation, as well as surface redox reactions on a photocatalyst.

clarified into collision and recombination. On one hand, the electrons and holes could reach the equilibrium state through their carrier–carrier collisions. On the other hand, the electrons and holes are recombined while releasing luminescence or heat to reach the equilibrium state [63]. Based on the discussion above, the incident intensity and band gap of photoelectrodes determine the theoretical power conversion conducted by photoactive semiconductor materials. Therefore, the optimization of band gaps is of huge significance to photoelectrodes, which could be achieved by density functional theory that is generally introduced to the design of band gaps. However, there might be inconsistency in predicting band gaps between theory and practice due to the limitation of density functional theory calculation in modeling [64]. Nevertheless, it is still a long-term and arduous task to explore semiconductor materials with appropriate band gaps for the PEC water splitting. From an experimental perspective, the band gap of semiconductor material could be optimized through not only the modification of materials' structures and compositions but also the doping method. Different from the alteration of composition, dopants in small amounts would not affect the bulk structure, but they could replace host atoms or remain at the interstitial site [64], to optimize the band gaps of bulk semiconductors. Furthermore, doping with two or more suitable elements might remarkably enhance the photocatalytic properties of a semiconductor material due to the synergistic effect between host elements and co-doping elements. This synergistic effect exerts a positive impact on the light absorption and the separation ability of the photogenerated electron-hole pairs [65,66].

5.2 Charge transportation

The charge separation will occur immediately after the electron-hole pairs are photogenerated. The positively charged holes and negatively charged electrons are attracted to each other by Coulomb attraction, thus being bonded together in space under certain conditions. The formed complex containing one hole and one electron is called an exciton. The Coulomb attraction between holes and electrons determines the spatial distribution and charge transportation. The electron-hole pair could be regarded as a free carrier when its wave function turns to be irrelevant. The heavier charge carriers demonstrate a smaller root mean square motion compared with lighter ones, implying that the lighter carriers could achieve much more effective charge separation [22,54,67]. The interface plays a key part in effective charge separation. Specifically, it stimulates the separation of electron-hole pairs in the form of *p*–*n* junctions. Due to the electrochemical potential differences between photoelectrodes and electrolytes, the space charge layer would be formed and the electrons would flow from the region with higher potential to that with lower potential. During the process, a compensating electric field is created by the aggregation of electrons to stop the backflow of electrons, causing a band bending of semiconductor materials. Theoretical studies have suggested that the band bending in a PEC system is heterogeneous and intensively distributed in the defect region [68−71].

In a PEC device, the contact area between the semiconductor material and liquid phase is the interface. The liquid phase occupies the mobile charge carriers, leading to the formation of a Schottky junction. As to the electrolyte, the charge is redistributed, resulting in the formation of the Helmholtz layer. In this case, the field of the semiconductor material might extend, which depends on the morphologies, compositions, and concentrations of dopants. It facilitates the charge separation and pushes the minority carriers to the surface to obtain excessive energy [69,71]. The more abundant charge carriers in semiconductors are defined as majority carriers (i.e., electrons and holes in *n*- and *p*-type semiconductors, respectively) while the fewer ones are termed minority carriers [4]. Given the above-mentioned field action of the semiconductor material, the charge carriers could finally reach the surface with excessive energy corresponding to a band bending level. Undesirable capture of charge carries is also likely to happen during the transport process. For example, when a hole or electron passes through the lattice of a semiconductor, it would be delocalized by the lattice over the surrounding atoms. Under this circumstance, the charge carrier would change the bond lengths and angles of semiconductors because the electron or hole will fill or empty the band with the bonding or antibonding properties of the lattice, respectively. If the charge carriers are delocalized on major atoms, the impact will be minimal. On the contrary, if the charge carriers are delocalized on minor atoms, the lattice will be tremendously distorted [72,73].

The charge recombination is an issue that needs to be overcome during the process of photogenerated charge carrier transportation. Both the charge separation and transportation depend on the crystal structure, degree of crystallinity, and the particle size of the semiconductor because the defective sites usually act as the trapping and recombination sites [74]. As a result, highly crystalline semiconductor materials with fewer defects have the potential to display higher photocatalytic activities theoretically. Besides, the nanosized materials generally possess a low recombination probability due to the short diffusion pathway for holes or electrons to reach the surface active sites. Furthermore, the high specific surface areas of nanosized materials are also conducive to the efficient interaction of surface active sites and charge carriers [6,74,75].

Apart from the influencing factors affecting the charge transportation discussed above, the electrolyte, the structure of defects, and the morphology of semiconductors also exert effects on the transportation of the photoge-

nerated charge carriers [76−78]. For example, nanotube-based semiconductor materials with one-dimensional structures possess direct transfer pathways, thus improving the charge transportation efficiency [79]. Another good example is the tandem PEC device consisting of a photoelectrode and a dye-sensitized solar cell (DSSC). Generally, a large surface area could improve the loading of dyes and the dye molecules combined with the transfer pathways in the nanotubes could further promote the electron-hole separation and the collection efficiency of charge carriers [80].

5.3 Charge utilization

After the transport process, charge carriers finally reach the active sites and are utilized to convert water molecules into H_2 and O_2. As discussed in section 2, for an effective semiconductor the potential of CB needs to be much more negative than the HER potential to trigger the water reduction while the potential of VB should be much more positive than the OER potential to trigger the water oxidation.

Surface redox reactions OER and HER have slow kinetics. To conquer the energy barrier of charge transfer, co-catalysts could be well dispersed on the surface of semiconductor materials to enhance the kinetics of the PEC redox reactions at interfaces. The addition of co-catalysts facilitates the fast charge transfer, thus decreasing the required overpotential for the water splitting reactions. In particular, OER triggered by the photo-excited holes is more kinetically sluggish due to the four-electron transfer process compared with HER, which restricts the overall water splitting efficiency. Therefore, the addition of co-catalysts is almost indispensable for OER photocatalysts. Noble metal Ru- and Ir-based materials and non-noble Ni-based (oxy-)hydroxides are often applied to the PEC devices as efficient co-catalysts for water oxidation [81].

In addition, the sacrificial agents could be employed to achieve a higher STH efficiency in PEC water splitting systems by improving the charge utilization and minimize the charge recombination. The sacrificial agents could serve as both hole and electron scavengers for hydrogen and oxygen evolution, respectively. The hole scavengers such as methanol could adsorb holes and are oxidized to CO_2. Meanwhile, the photoexcited electrons participate in water reduction with a prolonged lifetime. In contrast, electron scavengers such as silver nitrate adsorb electrons and are reduced, while the photoexcited holes take part in water oxidation [82].

In brief, the basic processes involved in the PEC water splitting are the creation of photogenerated electron-hole pairs, the charge carrier transportation, as well as the surface redox reactions. An in-depth understanding of these processes plays an essential role in the design of advanced photoelectrodes and efficient PEC devices to conduct the PEC water splitting.

6 Photoelectrode design

As a key component, photoelectrode could directly determine the overall performance of a PEC cell. Factors like the crystallinity, size, band gap properties, fabrication of photoelectrodes and other factors are closely related to highly efficient PEC water splitting [44,83,84].

6.1 Crystallinity

One of the essential properties of semiconductor materials is crystallinity. It has been observed that crystalline materials have higher efficiency than amorphous ones [45,59]. The increase in crystallinity could efficiently decrease defects in semiconductor materials that might be the recombination centers of electron-hole pairs. Therefore, the recombination rate of electrons and holes in crystalline photoelectrodes is significantly reduced, implying a higher efficiency of utilizing charge carriers to initiate redox reactions on the surface of photoelectrodes. For instance, TiO_2 nanorods attained crystallinity after annealing at 450 °C, showing better PEC performance with 5.2 times higher photocurrent density compared with pristine TiO_2 [85]. Notably, an ideal semiconductor material should possess not only a high degree of crystallinity but also a high specific surface area [86,87]. However, the degree of crystallinity of a semiconductor would increase with the decrease of the surface area or vice versa. Therefore, a compromise is needed to obtain optimal performance between crystallinity and the surface area of a semiconductor [59,88,89].

Moreover, the crystal change of semiconductors could also enhance the PEC performance by optimizing the electronic structure and semiconductor alignment. For instance, the fabricated polycrystalline Ta_3N_5 nanorods on a Ta substrate presented vertically nanorod arrays structure, as shown in Fig. 4 [90]. The photoelectrodes with one-dimensional morphology like vertically aligned nanorods which have a highly ordered crystallinity (Figs. 4 (a−e)) on conductive support showed good PEC performance. It achieved a half-cell STH efficiency of 2.72% at 0.89 V *vs.* RHE and a saturated photocurrent density of 9.95 $mA \cdot cm^{-2}$ at 1.05 V *vs.* RHE. Similarly, vertical $SrNbO_2N$ nanorod arrays were prepared in a facile hydrothermal process followed by a nitridation treatment for the PEC water splitting (Fig. 4(f)) [91]. The catalyst possessed a morphology of vertically aligned nanorods and high crystallinity. These structural properties facilitated the rapid generation and transportation of charge carriers. Thus, the vertically aligned $SrNbO_2N$ nanorod arrays reached 2.6 times higher photocurrent density of 1.3 $mA \cdot cm^{-2}$ at 1.23 V *vs.* RHE than the lower crystalline $SrNbO_2N$ nanoparticle under irradiation of AM 1.5 G simulated sunlight. Different from the former examples, Chen et al. [92] reported a disordered TiO_2 nanocrystal

which was synthesized by introducing disorders into the nanophase TiO_2 via hydrogenation. In detail, a highly crystallized TiO_2 was synthesized and subsequently placed in a sample chamber with a high-pressure hydrogen system of 20 bar at ~200 °C for 120 h, to obtain the disorder-engineered TiO_2 coated with ca. 1 nm disordered layer. The maximum VB energy level of the disorder-engineered TiO_2 had a blue shift of about −0.92 eV to the vacuum level. The as-synthesized disorder-engineered TiO_2 along with a sacrificial reagent showed an STH efficiency of ~24% with long-term operation stability for the PEC water splitting. The limited defects on the surface of disorder-engineered TiO_2 caused the localization of photogenerated holes and electrons to hinder the recombination and provided a high charge separation efficiency that accelerated the electron transfer to produce H_2, strongly proving that the PEC water splitting efficiency could be affected by the crystallinity of semiconductor materials.

6.2 Size

Apart from the crystallinity, the size of the semiconductor materials could also affect their PEC performance [93]. In general, the total surface areas of smaller semiconductors are larger when evaluated at the fixed amount of semiconductors. It is known that the specific surface area of photoelectrodes and the corresponding photo activities have a positive correlation [94,95]. In terms of catalysis, a larger surface area of materials indicates more active sites for the adsorption of reactants. In addition to the increased active sites, downsizing semiconductor materials could shorten the pathway of electron and charge transfer. Thus, the nanosized materials with a high specific surface area have been employed as photoelectrodes in PEC systems, which could provide massive active sites and short pathways for charge transfer to improve the carrier diffusion to the interface, thus boosting the solar energy conversion efficiency [45,84,96]. Moreover, the nanosized materials are more efficient in light absorption, whose surfaces could facilitate the antireflection and increase the light scattering to achieve longer optical path length of incident irradiation, thus increasing the utilization efficiency of light [97,98]. Besides, in nanostructured materials, the short diffusion length of charge carriers could also minimize the recombination of electrons and holes.

Despite that the nanoscale of materials shows positive effects as depicted, the charge separation ability would be adversely affected. Generally, the built-in electric field of the space charge layer near the semiconductor surface facilitates the charge separation and the thickness of the space charge layer depends on the particle size. However, the thin space charge layer of nanosized materials could be negligible, which leads to their compromised charge separation ability [48,86].

6.3 Band gap

Another advantage of semiconductor materials is that their band gaps allow them to absorb light of a wide range of wavelengths of the solar spectrum. The semiconductors with large band gaps are not suitable for absorbing the light energy with required intensities, causing poor

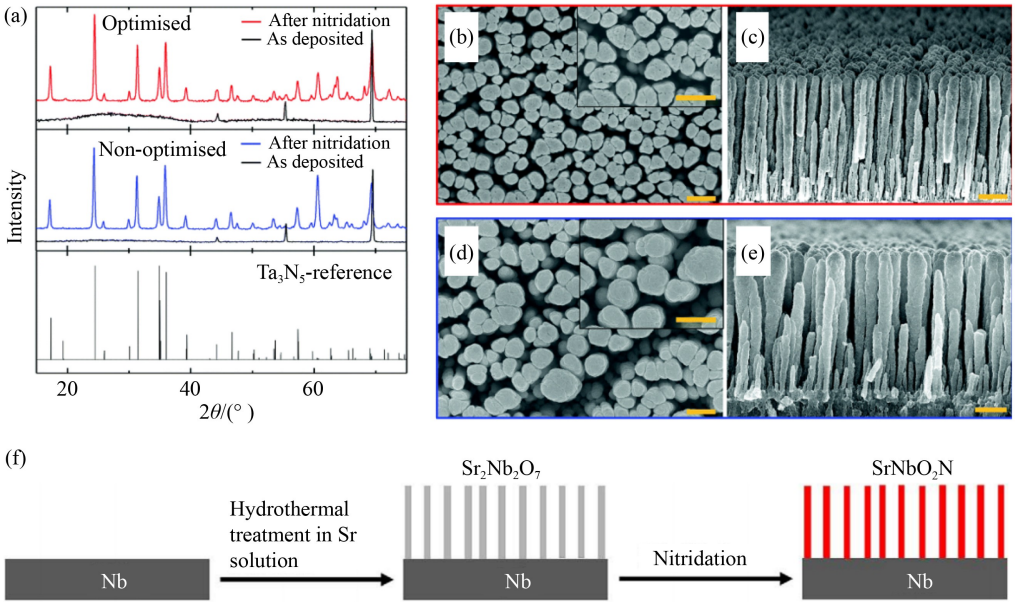

Fig. 4 The characterizations of structure and morphology for Ta/Ta_3N_5: (a) X-ray diffraction patterns and (b–e) scanning electron microscopy images of the top and cross-sectional areas of (b, c) the optimized and (d, e) non-optimized Ta/Ta_3N_5 nanorods. Reprinted with permission from Ref. [90], copyright 2020 Royal Society of Chemistry. (f) The synthetic routes for vertical $SrNbO_2N$ nanorod arrays. Reprinted with permission from Ref. [91], copyright 2021, Wiley-VCH.

PEC performance. Hence, the PEC performance will be improved accordingly if the band gap of the photoelectrode is narrowed. The suitable band gap for a highly efficient PEC water splitting should be within the range of 1.6−2.2 eV where the mobility of charge carriers and band edge position would be far more applicable [45]. In recent years, semiconductor materials including $BiVO_4$, Ta_2O_5, WO_3, CdS, TiO_2, etc. have been explored for the PEC water splitting, among which TiO_2 has been studied extensively due to its good photocatalytic activity, stability, low toxicity, and global availability. However, TiO_2 with a band gap of 3.2 eV is not suitable for the PEC water splitting as it only adsorbs 4% of sunlight in the UV light region and the recombination of charge carrier is quite fast [99,100]. Therefore, plenty of methods like element doping or coupling with visible light-responsive molecular catalysts have been adopted to reduce the band gap of semiconductors for efficient PEC performance [101,102]. The introduction of dopants to TiO_2 could shift its band gap towards the absorption in the visible light region by doping of TiO_2 with Ir, Co, Pt, and Fe or coupling with co-catalysts [81]. These strategies could lower the thermodynamic barrier, reduce the overpotential, and enhance the stability of precursor catalysts. In addition to mono-doping, the co-doping of cations and anions into TiO_2 materials could also improve the PEC performance of photocatalysts [103]. For instance, the tungsten and sulfur co-doped TiO_2 nanotubes showed superior photoelectrochemical performance [104]. An improved performance was observed by the co-doping of TiO_2 with metal and non-metal atoms which narrowed the band gap of TiO_2 and reduced the recombination of charge carriers. Similarly, the co-doping of TiO_2 with metals and S could enhance the photocatalytic activity of the catalyst, as was verified by the theoretical calculations [67]. These acceptor metals could facilitate the coupling of doped S and neighboring O to form an S−O bond, leading to the fully occupied energy levels in the forbidden band of TiO_2. This metal-assisted strategy could significantly reduce the band gaps of TiO_2 and prevent the recombination of the electron-hole pairs. Metal doping could enhance the light absorption ability by altering the energy levels of the semiconductor material, but sometimes metal dopants act as centers for the recombination of electrons and holes, which in turn decreases the charge separation efficiency.

Another strategy to overcome the drawback of wide-bandgap semiconductors is combining them with plasmonic metal materials like Au [105], Ag [106], Cu [107], and Al [108]. In an applied electric field induced by light, localized surface plasmon resonance is generated on the surface of these metals, i.e., hot electrons generated in metal materials are injected into the CB of semiconductors, leaving holes on the plasmonic particles used for the water splitting. Thus, the light absorption range of semiconductors is extended by the plasmonic metal particles [109,110]. Finely adjusting the shape [111−113], size [114], and composition [115,116] of plasmonic metal is likely to extend the light-adsorption range of photoelectrodes to cover the entire solar spectrum.

6.4 Fabrication of photoelectrodes

Photoelectrodes could be oxide or non-oxide semiconductors synthesized via various methods such as chemical vapor deposition, radio frequency, vacuum evaporation, and nitridation or sulphurization on conductive substrates. To obtain a good electric contact with substrates, powdered semiconductor materials are loaded on the conductive supports by electrophoretic deposition, drop-casting, and spin-coating, but the mechanical strength of such photoelectrodes is still not sufficient due to the resistance between substrates and particles. Therefore, necking treatments are introduced to enhance the interaction between conductive substrates and the semiconductor particles. Photoelectrodes containing powders are modified with metal salt precursor solutions and afterward annealed in an appropriate gas atmosphere. During the annealing process, the precursor metal salts are converted into the corresponding oxides or nitrides depending on the atmosphere, which bridge the semiconductor powders. Nevertheless, this necking strategy has certain limitations because some semiconductors and substrates are not stable during the annealing process or in a specific atmosphere (e.g., fluorine-doped SnO_2 in NH_3 atmosphere) [35,117,118].

An alternative particle transfer method is proposed to replace necking treatment. Specifically, a glass substrate is applied to support semiconductor powder before a thin metal layer of 100−300 nm is deposited to provide an electric contact. Thick metal films are deposited to enhance the mechanical strength and electric conductivity of photoelectrodes. Afterward, the primary glass substrate is peeled off and ultrasonication is applied to remove the excess powder. This method provides better electrical contact between the metal layer and the semiconducting particles, hence it is suitable for the fabrication of photoelectrodes with powdered semiconductors [35].

Another critical issue in photoelectrodes is the degradation mainly caused by the corrosion of photoelectrodes in highly acidic or alkaline electrolytes used to facilitate the water splitting reactions and eliminate the pH gradients resulting from inefficient ion diffusions at high current densities. Unfortunately, various semiconductors have poor chemical stabilities in these corrosive electrolytes under PEC operation conditions [119]. Therefore, protective layers have been deposited on semiconductors to minimize photoelectrode degradation and TiO_2 are widely adopted as chemically stable coatings to prevent direct contact semiconductors and electrolytes [120,121]. It features transparency and a wide potential window in pH = 0−14 electrolytes, almost ranging from 200 and

600 mV overpotentials with respect to the HER and OER, respectively [122]. Other protective layers such as Ni [123], NiO [124], CoO_x [125], Al_2O_3 [126], TiO_2/ZnO [127], and boron-doped diamond [128,129] are also explored for specific semiconductors and varied electrolytes. These protective layers have been deposited on semiconductors via physical vapor deposition, atomic layer deposition (ALD), chemical vapor deposition, and electrodeposition, to reduce the photoelectrode degradation to a negligible level.

6.5 Other factors

Apart from the factors mentioned above, the dimensionality of the semiconductor materials is also an influencing factor. The pH of electrolyte solutions determines the net charge on the surface of photoelectrodes and affects the equilibrium of the water splitting. Besides, other factors are also closely related to the PEC efficiency to conduct water splitting, such as temperature, pressure, as well as light sources [45,62,68,130]. For example, the construction of microstructured or nanostructured semiconductor materials has aroused wide concerns owing to its correlation with the STH efficiency of PEC devices. Generally, the category of semiconductor materials includes porous structure, zero-dimensional structure, one-dimensional structure, two-dimensional structure, and three-dimensional structure [45,68]. The semiconductor materials with porous structures facilitate the penetration of the electrolyte, which enlarges the contact area between electrolytes and photoelectrodes and decreases the transfer distance of charge carriers from semiconductors to surfaces. Compared with flat materials, light scattering is more likely to happen when light passes through the porous structures of the semiconductor materials. Moreover, the porous structure facilitates the charge separation and transport of the photogenerated holes and electrons [131]. The zero-dimensional materials such as quantum dots have efficient visible absorption abilities, excellent photocatalytic activities, as well as low electron-hole recombination rates [132−136]. This is because the small size of quantum dots is conducive to achieve a short transport distance of photogenerated holes and electrons from the bulk photoelectrode to the reaction interface and enhances the charge separation efficiency. More importantly, the quantum size effect of the semiconductor quantum dots will make the bottom of the CB and the top of the VB shift to higher reduction and oxidation positions, respectively, thus enlarging the band gaps of semiconductor quantum dots. Compared with two-dimensional materials, one-dimensional materials like nanorods, nanowires, and nanotubes tend to be more photoactive and favorable for charge carrier transport [48,137], especially nanotubes which possess a large surface area to boost the redox reaction rate [138,139]. Generally, one-dimensional structure features a small ratio of transverse to longitudinal size which is conducive to the rapid diffusion in a single direction, leading to low recombination of electron-hole pairs. In addition, one-dimensional structures could reduce specular reflection and allow the charge carriers to transfer along the longitudinal direction to the conductive substrate, thus enhancing the light absorption and the charge collection on the substrate. In contrast, two-dimensional structures such as nanosheets and macrosheets possess a high roughness, hence they have a reduced reflection of the incident light and an increased capturing capability of photons compared with the planar electrodes. Furthermore, two-dimensional semiconductor materials could harvest a large amount of UV light owing to their low thickness and large surface area, thus displaying an enhanced hydrogen generation efficiency. Interestingly, similar to the zero-dimensional quantum dots, the adjustment of redox and the band gap enlargement effect might occur when the thickness of two-dimensional nanostructures is lowered [140−142]. Three-dimensional materials could be formed, e.g., a dendritic structure composed of crosslinked one-dimensional nanowires, and an assembled and stacked structure composed of two-dimensional nanosheets [143,144]. Hence, three-dimensional semiconductors possess the features of one or two-dimensional materials with large surface areas. In particular, the interconnection of three-dimensional structures in diverse directions provides more pathways for charge transfer. In addition, the three-dimensional structures enhance light absorption by allowing for incident light reflection and refraction [145−148]. Consequently, the performance of photoelectrodes in three-dimensional structures is appealing.

7 Configurations of PEC devices

7.1 Single photoelectrode-based cell

The simplest PEC system is a single photoelectrode-based cell that only contains one semiconducting light absorber. The photoelectrode, which could be an *n*-type or *p*-type semiconductor, is employed as a photoanode or photocathode to conduct water oxidation or reduction, respectively. The commonly used photoanode materials are TiO_2, α-Fe_2O_3, $BiVO_4$, CdS, GaAs, and InP. While, Cu_2O, GaP, and Si are widely adopted as photocathodes [4]. As mentioned above, the energy bands of most semiconductors are not ideally positioned. To broaden the application scope of semiconductor materials, an external bias should be applied to compensate for the deficiency of potential required to conduct the redox reactions. These photoelectrodes can capture light and offer a significant amount of energy for the reactions and the externally applied electric/chemical bias provides the additional

voltage required for the reactions [102,149,150].

7.2 Z-scheme

The electronic properties of the semiconductor materials play a key role in enhancing the PEC water splitting performance of photoelectrodes. Thus, there is limited room for optimization as to the performance of the above single component PEC cell design. Nevertheless, considerable efforts have been made to enhance the efficiency of semiconductors to absorb light in a wide range of the solar spectrum, conceiving the idea of forming hetero-structure photocatalysts such as *p–p*, *n–n*, *p–n*, and *n–p* junctions. The hetero-junction structures (e.g., ZnO/Al_2O_3 [151], TiO_2/Al_2O_3 [152], and TiO_2/ZnO/boron nitride [129]) could reduce the recombination of charge carriers and assist in their movement and separation [30,43,59,153].

Natural photoelectrodes could be simulated utilizing two semiconductors photosynthesis, which is a design known as Z-scheme, as shown in Fig. 5. The Z-scheme system could perform photoexcitation with the reversible redox shuttles, in which one semiconductor is used for the oxidation of water to oxygen and the other for the reduction of water to H_2 [154]. The Z-scheme could enhance the transfer of charge carriers, which significantly improves the efficiency of the PEC water splitting. It is observed that the two-step Z-scheme could utilize visible light more efficiently than the conventional one-step process.

For example, Wang et al. [155] reported a Z-scheme system based on the ZnO/CdS heterostructure, which was applied to highly efficient PEC water splitting under simulated solar light irradiation. The as-prepared 1 wt% Pt-loaded $(ZnO)_1/(CdS)_{0.2}$ obtained 3870 $\mu mol \cdot h^{-1} \cdot g^{-1}$ for H_2 evolution. The excellent PEC water splitting performances with the lifetime of photoexcited carriers prolonged were attributed to the Z-scheme PEC system consisting of two closely contacted semiconductors. Meanwhile, an assorted Z-scheme comprising an O_2 production photoanode of $BiVO_4$ or WO_3 and a H_2 production photocathode of $Pt/SrTiO_3$:Rh was proposed by Kato et al. to decompose water into H_2 and O_2 under visible light irradiation, in which the H_2 evolution on the $Pt/SrTiO_3$:Rh photocatalyst was improved and the O_2 evolution was restrained by Fe^{2+} ions due to the oxidation of Fe^{2+} [156]. In this system, the PEC overall water splitting could be realized with the suppression of the back-reactions between H_2 and O_2, which could be ascribed to the novel Z-scheme system acting as not only

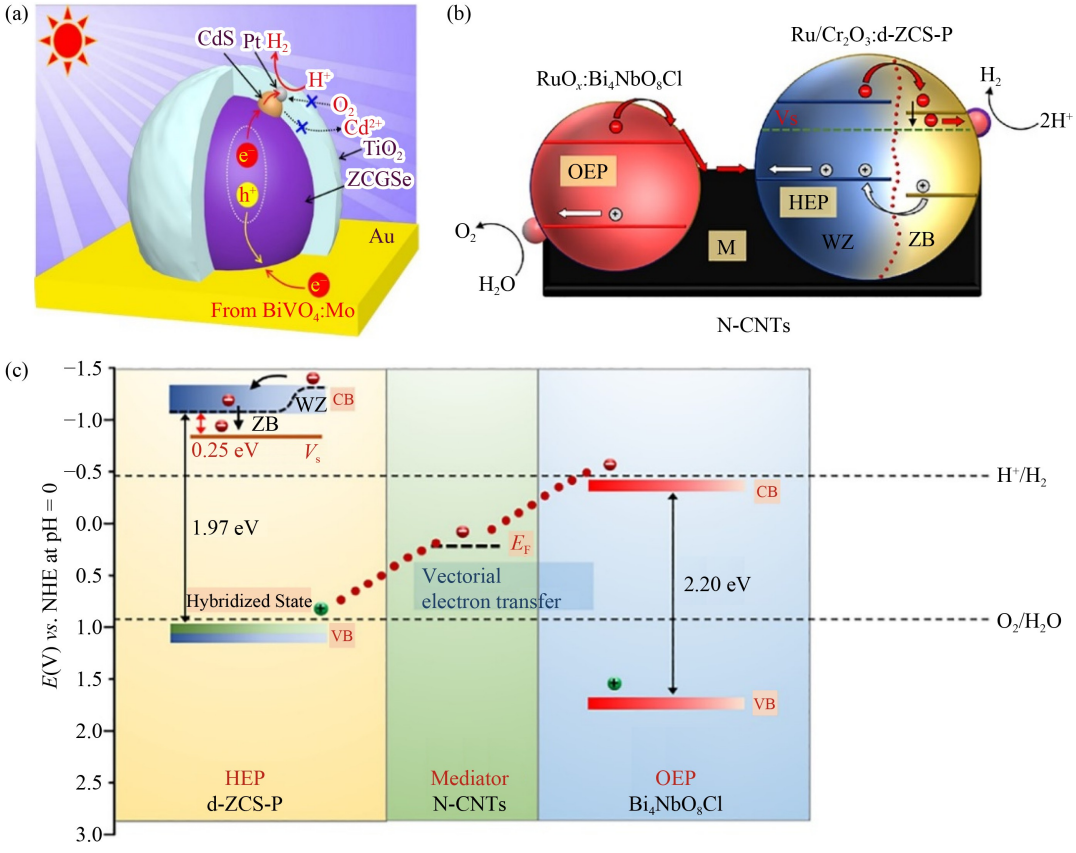

Fig. 5 (a) The suggested mechanism of photocatalytic process over Pt/TiO_2/CdS-ZCGSe/Au/$BiVO_4$:Mo. Reproduced with permission from Ref. [157], copyright 2021, American Chemical Society. (b) The mechanism for charge transportation in a Z-scheme system of d-ZCS-P/N-CNTs/Bi_4NbO_8Cl and (c) calculated band diagram. Reproduced with permission from Ref. [158], copyright 2021, Elsevier.

an inhibitor of the back-reactions but also an efficient electron mediator. In addition, a $(ZnSe)_{0.5}(CGSe)_{0.5}$/Au/$BiVO_4$:Mo based Z-scheme was constructed by applying a particle transfer method to the PEC overall water splitting (Fig. 5(a)) [157], in which $(ZnSe)_{0.5}(CGSe)_{0.5}$ material worked as an HER photocatalyst and Au/$BiVO_4$:Mo as an OER photocatalyst. The as-prepared Z-scheme system could obtain the highest quantum yield of 1.5% at 420 nm light range among all the reported metal sulfides/selenides Z-scheme photocatalysts. Similarly, P-doped twinned $Zn_{0.5}Cd_{0.5}S_{1-x}$ (d-ZCS-P)/N-doped carbon nanotubes (N-CNTs)/Bi_4NbO_8Cl-based Z-scheme photocatalysts were synthesized in a two-step procedure containing spray-coating and annealing treatment (Fig. 5(b)) [158]. The as-prepared photocatalysts achieved an STH efficiency of 0.15% under ambient conditions. Thus, it could be concluded that a well-constructed *p–n* junction system is suitable for conducting efficient charge separation which enhances the PEC performance. The characterization of the band structure is of huge significance to determining the corresponding fundamental electronic configuration and band symmetry, which aims at achieving deeper comprehension of the thermodynamic feasibility of the Z-scheme-based devices during the PEC water splitting and the impact on the conductive mediator. The d-ZCS-P possessed a band gap of 1.97 eV and the impurity level had a band gap of 0.25 eV below the CB, which could be calculated by the linearized form of the Urbach equation (Fig. 5(c)) [158]. Given the band gap of 2.2 eV displayed by Bi_4NbO_8Cl, a conclusion could be drawn that the Bi_4NbO_8Cl was visible-light active due to the exceedingly dispersive O 2p orbital that could narrow the band gap and enhance the electronegative VB. Recently, Wang and coworkers [159] designed and synthesized a series of ZnO/TiO_2-based core-shell heterostructures, the carrier lifetime of which was prolonged by ~20 times compared with the bare ZnO nanorods by time-resolved photoluminescence tests. More interestingly, the performance was further enhanced through employing Ag nanoparticles at the ZnO/TiO_2 interface to assemble a ZnO–Ag–TiO_2 Z-scheme structure. The innovative Z-scheme structural samples were subsequently integrated into a PEC cell to conduct the solar water splitting. The PEC cell achieved a photocurrent density jump over 5.5 mA·cm^{-2} in each circle, implying a photo-to-current efficiency of over 25% in the UV region. Under the visible light irradiation, the optimal Z-scheme structural sample displayed a high photocurrent density of 0.13 mA·cm^{-2}. The outstanding PEC performance demonstrated that the ZnO–Ag–TiO_2 nanorod array-based Z-scheme system could act as a prolonged carrier lifetime system for the PEC water splitting.

7.3 Tandem cell configuration

The tandem cell configuration is composed of series-connected photoanodes and photocathodes. This type of PEC tandem cell device possesses the advantages of increased photovoltage and diversiform selectivity of photoelectrode materials [29,56,160−162]. Initially, a semiconductor accompanied with a DSSC was used in a tandem device and applied to PEC water splitting [163]. Afterward, Kim et al. [164] proposed a tandem cell in which WO_3/Pt photoelectrode coupled with a DSSC for self-biased water splitting, as displayed in Fig. 6. The H:$Ti_3C_2T_x$/Cu_2O electrode was fabricated in two steps, i.e., the Cu_2O electrode was immersed into 0.3 mg·mL^{-1} of $Ti_3C_2T_x$ solution for 0.5 h and afterward annealed at 250 °C in Ar atmosphere for another 0.5 h (Fig. 6(a)) [165]. This system achieved an STH efficiency of 0.35%. Similarly, $Ti_3C_2T_x$/Cu_2O photocathode and $BiVO_4$/fluorine-doped tin oxide (FTO) photoanode were used in the tandem configuration, as illustrated in Fig. 6(b). The $Ti_3C_2T_x$/Cu_2O and $BiVO_4$/FTO tandem system achieved an STH efficiency of 0.55% (Fig. 6(c)). In this system, the light was first captured by the $Ti_3C_2T_x$/Cu_2O photocathode and then reached the $BiVO_4$/FTO photoanode. This novel configuration provided rapid charge transport and good light-harvesting ability that led to an improved STH efficiency in the tandem system.

Despite that the combination of DSSCs is considered as a promising PEC device configuration for solar water splitting, DSSCs are unable to generate sufficient voltage for water splitting, hence perovskite solar cells (PSCs) have been proposed due to their higher open-circuit voltage which is within the range of 0.9 to 1.5 V [166]. In this regard, a cobalt carbonate-catalyzed Mo-doped $BiVO_4$ photoanode and a $CH_3NH_3PbI_3$ PSC-based tandem configuration were proposed, which achieved a photocurrent density of 5 mA·cm^{-2} at 1.23 V *vs.* RHE [167]. This unique and stable wireless system configuration displayed an STH efficiency of 3.0%. Subsequently, a system composed of NiFe-layered double hydroxides and organohalide $CH_3NH_3PbI_3$ based-PSCs without an external energy supply was introduced [168]. The as-prepared system provided a photocurrent density of ~10 mA·cm^{-2} with an STH efficiency of 12.3%. Undoubtedly, this configuration provided a good PEC water splitting performance but the photoelectrodes were not effectively involved in redox reactions. Thus, H_2 production was conducted by a water electrolysis process in which electrical power was generated by two externally wired PSCs in series. Although such tandem solar cell-based systems have provided high photocurrent density, the stability of dyes and organohalide perovskites in the corresponding DSSCs and PSCs and efficient photon utilization have to be taken into consideration in these design concepts.

As known, the photoanode $BiVO_4$ has been regarded as one of the most favorable photoanodes for PEC water splitting, which could deliver a theoretical photocurrent density of 7.5 mA·cm^{-2} corresponding to an STH efficiency of 9.2% under AM 1.5 G illumination [169].

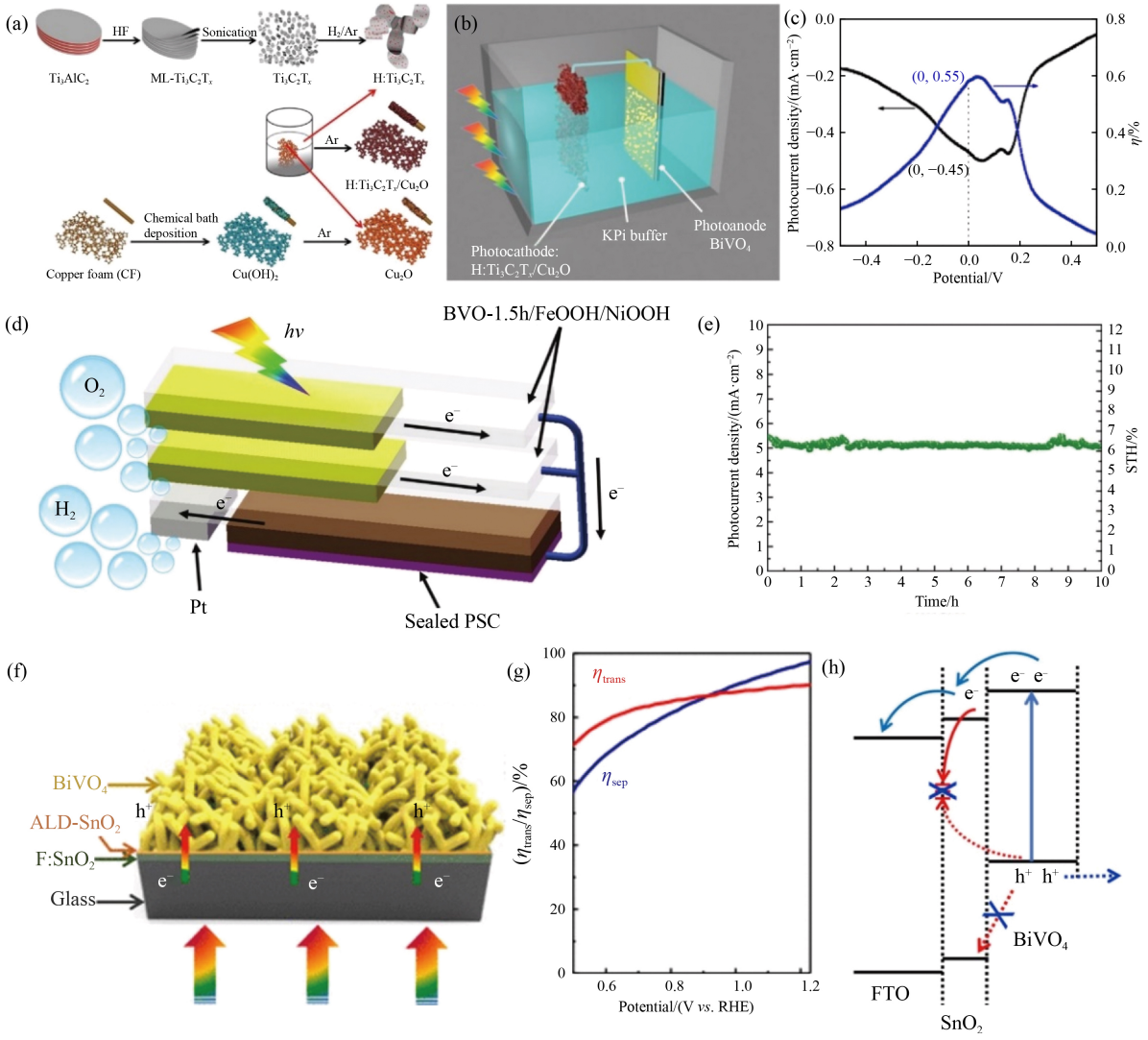

Fig. 6 Schematic diagrams of (a) synthesis method of H:$Ti_3C_2T_x$/Cu_2O photocathode, (b) a tandem solar-driven water splitting device, and (c) STH efficiencies under irradiation of AM 1.5 G simulated sunlight. Reprinted with permission from Ref. [165], copyright 2020, Elsevier. (d) Schematic structure of 2-BVO-FeOOH/NiOOH dual photoanodes coupled with a sealed PSC and (e) stability test of the unassisted water splitting as well as the corresponding STH value. Reprinted with permission from Ref. [169], copyright 2018, Wiley-VCH. (f) Schematic hierarchical structure of $BiVO_4$, (g) the experimental charge separation and transport efficiencies and (h) mitigation for charge recombination of $BiVO_4$ with a SnO_2 layer. Reprinted with permission from Ref. [170], copyright 2021, American Chemical Society.

The $BiVO_4$ has a marginally larger band gap than the ideal one (2.4 eV) which is required for the PEC water splitting. However, the CB edge position of $BiVO_4$ is almost equal to the H_2 evolution potential, which leads to a high photocurrent density and low onset potential compared with other photoanode materials. In this respect, a high-performance photoanode of oxygen vacancy-rich $BiVO_4$ was prepared by applying an electrodeposition method followed by a calcination process for the PEC water splitting (Figs. 6(d−e)) [169]. The $BiVO_4$ film-based photoanodes achieved a photocurrent density of 2.38 mA·cm^{-2} at 1.23 V *vs.* RHE under AM 1.5 G illumination in Na_2SO_3 electrolyte. Moreover, to enhance the kinetic of OER, the $BiVO_4$ photoanodes were loaded with an amorphous FeOOH/NiOOH layer, displaying an outstanding photocurrent density of 5.13 mA·cm^{-2} at 1.23 V *vs.* RHE under AM 1.5 G illumination for the PEC water splitting. The high performance was attributed to the presence of oxygen vacancies in the structure of the $BiVO_4$ photoanode, which were supposed to improve the carrier density and charge separation efficiency of $BiVO_4$. In addition, the $BiVO_4$ has a rapid electron-hole recombination behavior and lower carrier mobility, which are caused by the inefficient charge transport pathways. Therefore, the morphology control including shape, connectivity of a semiconductor material, and dimension has been applied to refine the unbalanced charge transport kinetics. For example, the hierarchical morphology of a photoelectrode offers a large surface area, which facilitates charge transport and balanced charge separation and

subsequently increases the overall quantum efficiency of the PEC system. Thus, orientation engineering was applied to fabricate hierarchical $BiVO_4$ [170]. A solvothermal method was employed to prepare the precursor materials in various morphologies by controlling the solvent proportion of ethylene glycol to ethanol, after which the targeted $BiVO_4$ in hierarchical morphology was formed by chemical treatment in the following heating process (Fig. 6(f)). This unique structure was composed of voids and highly exposed active sites, hence large interfacial areas were provided to ensure sufficient contacts with the electrolyte, contributing to the enhanced PEC properties in terms of charge separation and transport efficiency (Figs. 6(g–h)). In addition, the performance of hierarchical $BiVO_4$ was further enhanced by depositing an 8 nm SnO_2 layer, an ultrathin layer which could increase the charge collection efficiency and restrict the recombination of holes and electrons. When the material was applied to the PEC water splitting, the results displayed a charge separation efficiency of 97.1% and charge transport efficiency of 90.1% at 1.23 V *vs.* RHE which were the highest ones among $BiVO_4$-based photoanodes for OER.

In addition to morphology changes, the effect of elemental doping and hetero-junction formation on the performance of $BiVO_4$ has also been evaluated for the PEC water splitting. In this respect, the Mo-doped $BiVO_4$ was firstly prepared with different amounts of doped Mo [27]. In pure $BiVO_4$, the Fermi-level pinning effect inhibited the tuning of quasi-Fermi-level close to the CB minimum that resulted in a low open-circuit voltage. This side effect could be suppressed by Mo doping. Suitable doped Mo in $BiVO_4$ could shift the Fermi-level to a positive direction and quasi-Fermi-level to a negative direction. Thus, the open-circuit voltage was enlarged from −0.35 to −1 V in the case of 0.1% Mo doped $BiVO_4$. This operation also focused on the construction of a hetero-junction composed of boron-doping C_3N_4 and Mo-doped $BiVO_4$. This hetero-junction showed a stronger absorption ability in the range of 300−500 nm than Mo-doped $BiVO_4$. The boron-C_3N_4/Mo-$BiVO_4$ photoanode had witnessed a significant improvement in their performance by achieving photocurrent densities of 4.7 and 6.0 $mA \cdot cm^{-2}$ at 0.6 and 1.23 V *vs.* RHE, respectively in a buffer solution with 0.5 $mol \cdot L^{-1}$ Na_2SO_3 hole scavenger. Moreover, the $NiFeO_x$/B-C_3N_4/Mo-$BiVO_4$ photoanode was prepared by anchoring $NiFeO_x$ on the surface of BC_3N_4/Mo-$BiVO_4$ to perform OER. The as-prepared catalyst showed photocurrent densities of 3.85 and 5.93 $mA \cdot cm^{-2}$ at 0.54 and 1.23 V *vs.* RHE respectively. More importantly, the highest IPCE of 92% was attained during the PEC process at pH = 7. The results were better than the reported $BiVO_4$-based PEC devices to date. Notably, the $NiFeO_x$/B-C_3N_4/Mo-$BiVO_4$ photoanode was highly stable, showing negligible changes in its performance after 10 h operation. Conclusively, the synergistic combination of doping and hetero-junction played a critical part in providing the remarkable PEC performance of $NiFeO_x$/B-C_3N_4/Mo-$BiVO_4$ photoanode.

7.4 Monolithic design

A novel monolithic design is applied to tandem cells. The monolithic design-based devices with leaf-like structures are wireless and sheet-like, which could operate without external bias. Compared with wired devices, they usually display lower STH efficiencies due to their less intimate contact. However, the monolithic design is an effective strategy for the device construction in small size due to its simple configuration [30], supported by samples in Fig. 7. In this aspect, a *p–n* junction photoelectrode containing *n*-type TiO_2 nanotube arrays and *p*-type Cu−Ti−O was investigated for the PEC water splitting. The as-prepared system had only a minimal amount of photo corrosion at Cu−Ti−O photocathode after 4−5 h operation in 0.1 $mol \cdot L^{-1}$ Na_2HPO_4 electrolyte [171]. Meanwhile, Oh and coworkers [172] reported a monolithic architecture by locally fabricating an ordered three-dimensional porous NiFe inverse opal on a Si photoanode to decouple light absorption and OER process. It could allow for more light absorption and offer more electrochemically active sites, thus greatly enhancing O_2 evolution. The optimal Si-based photoanode with NiFe alloy inverse opal displayed a stable photocurrent density of 31.2 $mA \cdot cm^{-2}$ at 1.23 V *vs.* RHE in 1 $mol \cdot L^{-1}$ KOH under 1 sun illumination. Ganesh et al. [173] reported another monolithic InGaN/GaN multi-quantum well structure, which was fabricated on the sapphire substrate at different growth temperatures via the metal-organic chemical vapor deposition method. The as-synthesized monolithic InGaN/GaN multi-quantum well structures were proved to possess an appropriate surface morphology, periodicity built by InGaN/GaN well and barrier layers, indium concentration, as well as optical band gap, which enhanced PEC performance. This further demonstrated the superiority of monolithic design for the PEC water splitting. Very recently, Zhu et al. [174] reported a monolithic solar water splitting device, where the photoanode was fabricated by a series of novel double perovskite cobaltites with high efficiency of OER in alkaline solution while the photocathode was a NiMo catalyst. The PEC device based on the monolithic design showed an STH efficiency of 6.6% in 1.0 $mol \cdot L^{-1}$ NaOH under uninterrupted one-sun simulated illumination for 71 h. In another study, a monolithic photoanode device consisting of core-shell *n*-Si/SiO_x/TiO_2/WO_3/$BiVO_4$ hetero-junctions was developed via the chemical deposition method (Fig. 7(a)) [175]. TiO_2 acted as a buffer layer to passivate the *n*-Si/SiO_x surfaces, thus forming fewer interface states. This was demonstrated by the band diagrams shown in Fig. 7(b). In the case of *n*-Si/SiO_x/WO_3, the interface states might locate below the bulk Fermi level of WO_3. During the

formation process of the hetero-junction, the Fermi levels of WO_3 and *n*-Si struck a balance with the defect states, which caused the band bending upward with a depletion region at the surfaces of WO_3 and *n*-Si. Thus, the *n*-Si/SiO_x/WO_3 junction displayed an electron energy barrier of 0.5 eV and only at high reverse bias could the interfacial barrier be conquered. It is noteworthy that the surfaces of *n*-Si/SiO_x passivated by TiO_2 led to a lower energy barrier for electrons at the interfaces of metal oxides (Fig. 7(c)). The as-prepared system could split water without an external bias and showed an STH efficiency of 0.37% (equal to a maximum photocurrent density of 0.3 mA·cm^{-2}). Meanwhile, a monolithically integrated device based on InGaN/Si double-junction photocathode was developed to perform highly efficient and stable unassisted solar water splitting (Figs. 7(d−f)) [176]. The InGaN nanowire tunnel junction was formed by a monolithic incorporation of *p*-type InGaN top junction on an underlying Si *p*–*n* junction. This monolithically integrated system obtained an STH efficiency of 10.3% in an acid electrolyte with the help of Pt catalysts and atomic Al_2O_3 passivation layer. Given the above, PEC devices could achieve high STH efficiencies and prolonged operating time through rational monolithic design. However, the complexity of the fabrication process and high cost have hindered the commercialization of this water splitting system.

8 Summary and perspectives

With the rapid progress of modern science and technology, solar-driven water splitting has witnessed explosive development to meet the rising demand for sustainable hydrogen production in recent years. This review presented the elementary but significant mechanisms

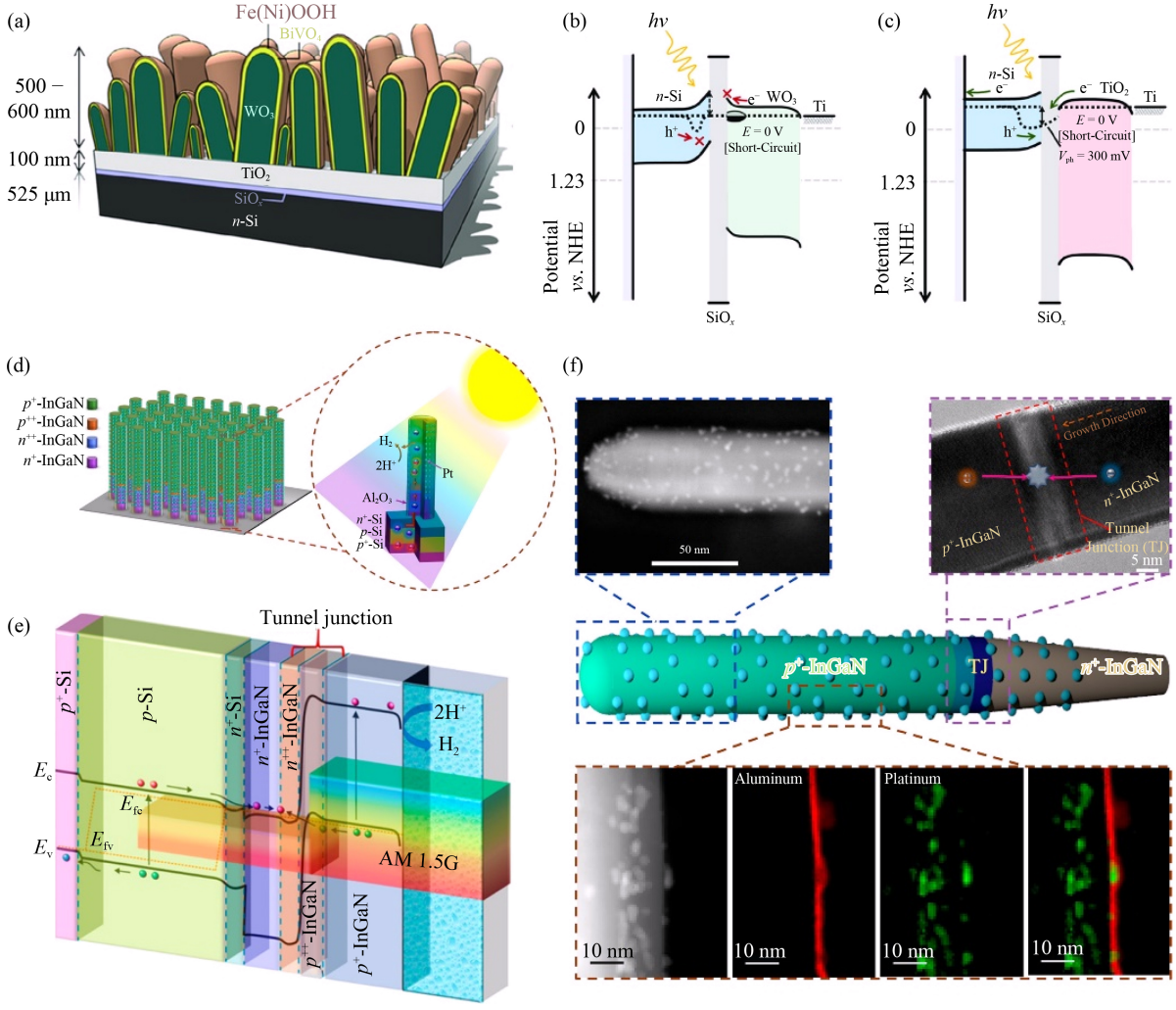

Fig. 7 (a) Schematic illustration of the *n*-type TiO_2/*p*-type Cu–Ti–O nanotube arrays architecture and estimated band diagrams of (b) *n*-Si/SiO_x/WO_3/Ti and (c) *n*-Si/SiO_x/TiO_2/Ti hetero-junctions. Reprinted with permission from Ref. [175], copyright 2020, Wiley-VCH. (d) The InGaN nanowire arrays on Si substrate after deposition of Al_2O_3 and Pt, (e) band diagram of the InGaN/Si photocathode and (f) the structure of surface-modified InGaN nanowire. Reprinted with permission from Ref. [176], copyright 2020, American Chemical Society.

involved in the PEC water splitting. The major electrochemical processes have been summarized, especially the compact correlation between the electronic properties of photoelectrodes and the PEC water splitting efficiency. Moreover, the general parameters to evaluate the PEC device performances for HER and OER reactions have been concluded, including STH efficiency, Faradaic efficiency, and IPCE. A fundamental understanding of the PEC water splitting plays a significant role in the design and fabrication of a photoelectrode, which is the main component of PEC systems with the function of light absorption. Therefore, the intrinsic charge generation, transportation, and utilization processes which occur on the photoelectrodes and at the interfaces of semiconductor materials and electrolytes have been discussed. Furthermore, the factors influencing the orderliness, uniformity, and morphology of photoelectrodes which affect the PEC efficiency for water splitting including crystallinity, size, band gap, and the fabrication process have been introduced. Finally, the recent advances in PEC hydrogen production systems have also been reviewed. In this regard, diverse configurations of PEC devices have been described, e.g., the basic single photoelectrode-based cell, the Z-scheme-based PEC device, the tandem PEC device, as well as the monolithic PEC water splitting device.

Despite the achievements made in the design of various semiconductor materials for integration into advanced solar-driven water splitting devices to produce hydrogen over the past decades, the reported STH efficiencies for the PEC water splitting are still insufficient for commercial applications. To obtain a satisfactory STH efficiency, the PEC water splitting device should possess a good photoresponse performance in a wide range with efficient charge separation and transportation, long-term operation stability, as well as fast kinetics in the half-reactions of water splitting. To this end, the following directions of future research on the design and fabrication of appropriate photoelectrodes and PEC systems will be of certain guiding significance:

1) The PEC water splitting process involves light absorption of semiconductors and complicated charge photogeneration and separation processes, surface redox reactions, and so on. The insight into the water redox mechanisms is crucial to improving the PEC water performance for practical application. To this end, the advanced characterization techniques such as transient absorption spectral measurements, X-ray absorption spectra, Fourier transform infrared spectroscopy, X-ray photoelectron spectroscopy, and their operando or *in situ* spectroscopy experiments could be employed to clarify the dynamic behaviors (e.g., valence states and the composition and nature of active sites) as well as the interfacial charge transportation and surface reactivity. In addition, the ultra-fast spectroscopies which could deliver essential information in a very short time are required for investigating the PEC water splitting mechanisms. The resultant information could guide rational designs on semiconductors and co-catalysts.

2) The saturated photocurrent density is generally determined by the number of absorbed photons while charge separation and utilization depend on the diffusion distance of charge carriers. Therefore, it is an effective strategy to design and fabricate the photoelectrodes using economic and effective materials with a wide light absorption range and long carrier diffusion distance. Moreover, the energy band structure of semiconductor materials should match well with the electronic properties to guarantee photogenerated charge transportation. Thus, appropriate active electrocatalysts should be applied to cater to the sub-layered semiconductors when the photoelectrodes are fabricated. More importantly, the interlayer between the electrocatalyst and semiconductors should be optimized and the series resistance for charge transfer from semiconductor to electrocatalyst should be decreased. Advanced semiconductors with a wide range of light absorption, progressive methods for enhancing charge separation, as well as novel techniques for gas separation should be explored urgently to realize the scaled-up solar hydrogen production.

3) As for the PEC devices, various innovations concerning materials, architecture design, and co-catalyst optimization have been made in recent years to boost the activity. However, the long-term stability of a PEC device should be further improved, which is critical in practical industrial application. Although protective layers have been coated to construct chemical stable photoelectrodes in harsh electrolytes, the process of coating engineering should still be seriously taken into account. For example, solution processing is low-cost and versatile to grow films, but the uncontrollable nucleation and growth process results in a shorter lifetime and poorer quality of films, which show a continuous cover without cracked surface and uniform thickness. On the contrary, the ALD technique could control the thickness of films at the atomic level and produce superior high-quality films. However, this promising film processing technique is hindered by limited compositions for depositions, high cost in devices, and obstacles to depositing large-scale films. Besides, after the coating of protective layers, a deeper understanding of newly created interfaces should also be exploited to minimize carrier loss. These findings will shed light on the other PEC fields such as CO_2 photoreduction, N_2 fixation, and pollutants removal.

Besides, new designs in Z-scheme or monolithic devices should be developed to meet the requirements of various semiconductor materials assembled in a PEC water splitting device. Last but not least, a standardized test should be designed to guarantee the repeatability of the PEC device efficiencies, which are alterable under different experimental setups and conditions. The highly reproducible performance, coupled with the upgrading of photoelectrodes' fabrications, is essential for the

commercialization of PEC devices. More efforts should be devoted to the development of low-cost large-scale fabrication methods with highly reproducible results. Nevertheless, considerable progress has been made in both advanced photoelectrodes and novel PEC device design to date. It is inspiring that the scientific research field of solar-driven water splitting is bound to move forward and eventually be applied to industrial application.

Acknowledgements Yang Hou acknowledges the funding supports from the National Natural Science Foundation of China (Grant Nos. 2196116074, 21878270, and 221922811), Fundamental Research Funds for the Central Universities (Grant No. 2020XZZX002-09), Zhejiang Provincial Natural Science Foundation of China (Grant No. LR19B060002), Startup Foundation for Hundred-Talent Program of Zhejiang University, Zhejiang Key Laboratory of Marine Materials and Protective Technologies (Grant No. 2020K10), Jiangxi Province "Double Thousand Plan" project (Grant No. 205201000020), Key Laboratory of Marine Materials and Related Technologies, CAS, and the Leading Innovative and Entrepreneur Team Introduction Program of Zhejiang (Grant No. 2019R01006). Zhibin Liu acknowledges the funding support of the Research Funds of Institute of Zhejiang University-Quzhou.

References

1. Shi P, Cheng X, Lyu S. Efficient electrocatalytic oxygen evolution at ultra-high current densities over 3D Fe, N doped $Ni(OH)_2$ nanosheets. Chinese Chemical Letters, 2021, 32(3): 1210–1214
2. Wang K, Wang X, Li Z, Yang B, Ling M, Gao X, Lu J, Shi Q, Lei L, Wu G, Hou Y. Designing 3d dual transition metal electrocatalysts for oxygen evolution reaction in alkaline electrolyte: beyond oxides. Nano Energy, 2020, 77: 105162
3. Kannan N, Vakeesan D. Solar energy for future world: a review. Renewable & Sustainable Energy Reviews, 2016, 62: 1092–1105
4. Jiang C, Moniz S J A, Wang A, Zhang T, Tang J. Photoelectrochemical devices for solar water splitting—materials and challenges. Chemical Society Reviews, 2017, 46(15): 4645–4660
5. Zhao Y, Ding C, Zhu J, Qin W, Tao X, Fan F, Li R, Li C. A hydrogen farm strategy for scalable solar hydrogen production with particulate photocatalysts. Angewandte Chemie International Edition, 2020, 59(24): 9653–9658
6. Kudo A, Miseki Y. Heterogeneous photocatalyst materials for water splitting. Chemical Society Reviews, 2009, 38(1): 253–278
7. Chang X, Wang T, Gong J. CO_2 photo-reduction: insights into CO_2 activation and reaction on surfaces of photocatalysts. Energy & Environmental Science, 2016, 9(7): 2177–2196
8. Kojima A, Teshima K, Shirai Y, Miyasaka T. Organometal halide perovskites as visible-light sensitizers for photovoltaic cells. Journal of the American Chemical Society, 2009, 131(17): 6050–6051
9. Grätzel M. Photoelectrochemical cells. Nature, 2001, 414(6861): 338–344
10. Choudhury C, Andersen S L, Rekstad J. A solar air heater for low temperature applications. Solar Energy, 1988, 40(4): 335–343
11. Cheng F, Wang L, Wang H, Lei C, Yang B, Li Z, Zhang Q, Lei L, Wang S, Hou Y. Boosting alkaline hydrogen evolution and Zn-H_2O cell induced by interfacial electron transfer. Nano Energy, 2020, 71: 104621
12. Lei C, Chen H, Cao J, Yang J, Qiu M, Xia Y, Yuan C, Yang B, Li Z, Zhang X, et al. Fe-N_4 sites embedded into carbon nanofiber integrated with electrochemically exfoliated graphene for oxygen evolution in acidic medium. Advanced Energy Materials, 2018, 8(26): 1801912
13. Lei C, Wang Y, Hou Y, Liu P, Yang J, Zhang T, Zhuang X, Chen M, Yang B, Lei L, et al. Efficient alkaline hydrogen evolution on atomically dispersed Ni-N_x species anchored porous carbon with embedded Ni nanoparticles by accelerating water dissociation kinetics. Energy & Environmental Science, 2019, 12(1): 149–156
14. Wang L, Li Z, Wang K, Dai Q, Lei C, Yang B, Zhang Q, Lei L, Leung M K H, Hou Y. Tuning d-band center of tungsten carbide via Mo doping for efficient hydrogen evolution and Zn-H_2O cell over a wide pH range. Nano Energy, 2020, 74: 104850
15. Hou Y, Qiu M, Kim M G, Liu P, Nam G, Zhang T, Zhuang X, Yang B, Cho J, Chen M, et al. Atomically dispersed nickel-nitrogen-sulfur species anchored on porous carbon nanosheets for efficient water oxidation. Nature Communications, 2019, 10(1): 1392
16. Hou Y, Qiu M, Nam G, Kim M G, Zhang T, Liu K, Zhuang X, Cho J, Yuan C, Feng X. Integrated hierarchical cobalt sulfide/nickel selenide hybrid nanosheets as an efficient three-dimensional electrode for electrochemical and photoelectrochemical water splitting. Nano Letters, 2017, 17(7): 4202–4209
17. Hou Y, Qiu M, Zhang T, Ma J, Liu S, Zhuang X, Yuan C, Feng X. Efficient electrochemical and photoelectrochemical water splitting by a 3D nanostructured carbon supported on flexible exfoliated graphene foil. Advanced Materials, 2017, 29(3): 1604480
18. White J L, Baruch M F, Pander J E III, Hu Y, Fortmeyer I C, Park J E, Zhang T, Liao K, Gu J, Yan Y, et al. Light-driven heterogeneous reduction of carbon dioxide: photocatalysts and photoelectrodes. Chemical Reviews, 2015, 115(23): 12888–12935
19. Niu F, Wang D, Li F, Liu Y, Shen S, Meyer T J. Hybrid photoelectrochemical water splitting systems: from interface design to system assembly. Advanced Energy Materials, 2019, 10(11): 1900399
20. Siavash Moakhar R, Hosseini-Hosseinabad S M, Masudy-Panah S, Seza A, Jalali M, Fallah-Arani H, Dabir F, Gholipour S, Abdi Y, Bagheri-Hariri M, et al. Photoelectrochemical water-splitting using CuO-based electrodes for hydrogen production: a review. Advanced Materials, 2021, 33(33): 2007285
21. Fujishima A, Honda K. Electrochemical photolysis of water at a semiconductor electrode. Nature, 1972, 238(5358): 37–38
22. Hellman A, Wang B. First-principles view on photoelectrochemistry: water-splitting as case study. Inorganics, 2017, 5(2): 37
23. Zhang H, Wang H Z, Xuan J. Rational design of

photoelectrochemical cells towards bias-free water splitting: thermodynamic and kinetic insights. Journal of Power Sources, 2020, 462: 228113

24. Zhang X Q, Bieberle-Hutter A. Modeling and simulations in photoelectrochemical water oxidation: from single level to multiscale modeling. ChemSusChem, 2016, 9(11): 1223–1242
25. Boumeriame H, Da Silva E S, Cherevan A S, Chafik T, Faria J L, Eder D. Layered double hydroxide (LDH)-based materials: a mini-review on strategies to improve the performance for photocatalytic water splitting. Journal of Energy Chemistry, 2022, 64: 406–431
26. Reddy C V, Reddy I N, Harish V V N, Reddy K R, Shetti N P, Shim J, Aminabhavi T M. Efficient removal of toxic organic dyes and photoelectrochemical properties of iron-doped zirconia nanoparticles. Chemosphere, 2020, 239: 124766
27. Ye K H, Li H B, Huang D, Xiao S, Qiu W T, Li M Y, Hu Y W, Mai W J, Ji H B, Yang S H. Enhancing photoelectrochemical water splitting by combining work function tuning and heterojunction engineering. Nature Communications, 2019, 10(1): 3687
28. Chandrasekaran S, Yao L, Deng L B, Bowen C, Zhang Y, Chen S M, Lin Z Q, Peng F, Zhang P X. Recent advances in metal sulfides: from controlled fabrication to electrocatalytic, photocatalytic and photoelectrochemical water splitting and beyond. Chemical Society Reviews, 2019, 48(15): 4178–4280
29. Chen Y B, Zheng W Y, Murcia-Lopez S, Lv F, Morante J R, Vayssieres L, Burda C. Light management in photoelectrochemical water splitting—from materials to device engineering. Journal of Materials Chemistry. C, Materials for Optical and Electronic Devices, 2021, 9(11): 3726–3748
30. Kim J H, Hansora D, Sharma P, Jang J W, Lee J S. Toward practical solar hydrogen production—an artificial photosynthetic leaf-to-farm challenge. Chemical Society Reviews, 2019, 48(7): 1908–1971
31. Li L Z, Liu C H, Qiu Y Y, Mitsuzak N, Chen Z D. Convex-nanorods of alpha-Fe_2O_3/CQDs heterojunction photoanode synthesized by a facile hydrothermal method for highly efficient water oxidation. International Journal of Hydrogen Energy, 2017, 42(31): 19654–19663
32. Wang C Z, Chen Z, Jin H B, Cao C B, Li J B, Mi Z T. Enhancing visible-light photoelectrochemical water splitting through transition-metal doped TiO_2 nanorod arrays. Journal of Materials Chemistry A, 2014, 2(42): 17820–17827
33. Varadhan P, Fu H C, Priante D, Retamal J R D, Zhao C, Ebaid M, Ng T K, Ajia I, Mitra S, Roqan I S, et al. Surface passivation of GaN nanowires for enhanced photoelectrochemical water-splitting. Nano Letters, 2017, 17(3): 1520–1528
34. Nie Q, Yang L, Cao C, Zeng Y M, Wang G Z, Wang C Z, Lin S W. Interface optimization of ZnO nanorod/CdS quantum dots heterostructure by a facile two-step low-temperature thermal treatment for improved photoelectrochemical water splitting. Chemical Engineering Journal, 2017, 325: 151–159
35. Hisatomi T, Kubota J, Domen K. Recent advances in semiconductors for photocatalytic and photoelectrochemical water splitting. Chemical Society Reviews, 2014, 43(22): 7520–7535
36. Hamdani I R, Bhaskarwar A N. Recent progress in material selection and device designs for photoelectrochemical water-splitting. Renewable & Sustainable Energy Reviews, 2021, 138: 110503
37. Li J K, Cheng K W. Surface modification of the *p*-type Cu_2ZnSnS_4 photocathode with *n*-type zinc oxide nanorods for photo-driven salt water splitting. International Journal of Hydrogen Energy, 2021, 46(53): 26961–26975
38. Li Z S, Luo W J, Zhang M L, Feng J Y, Zou Z G. Photoelectrochemical cells for solar hydrogen production: current state of promising photoelectrodes, methods to improve their properties, and outlook. Energy & Environmental Science, 2013, 6(2): 347–370
39. Wu N Q. Plasmonic metal-semiconductor photocatalysts and photoelectrochemical cells: a review. Nanoscale, 2018, 10(6): 2679–2696
40. Kim J H, Lee J S. Elaborately modified $BiVO_4$ photoanodes for solar water splitting. Advanced Materials, 2019, 31(20): 1806938
41. Saraswat S K, Rodene D D, Gupta R B. Recent advancements in semiconductor materials for photoelectrochemical water splitting for hydrogen production using visible light. Renewable & Sustainable Energy Reviews, 2018, 89: 228–248
42. Chen F, Ma T Y, Zhang T R, Zhang Y H, Huang H W. Atomic-level charge separation strategies in semiconductor-based photocatalysts. Advanced Materials, 2021, 33(10): 2005256
43. Qian W Q, Xu S W, Zhang X M, Li C B, Yang W Y, Bowen C R, Yang Y. Differences and similarities of photocatalysis and electrocatalysis in two-dimensional nanomaterials: strategies, traps, applications and challenges. Nano-Micro Letters, 2021, 13(1): 156
44. Zhang S, Ye H, Hua J, Tian H. Recent advances in dye-sensitized photoelectrochemical cells for water splitting. EnergyChem, 2019, 1(3): 100015
45. Joy J, Mathew J, George S C. Nanomaterials for photoelectrochemical water splitting—review. International Journal of Hydrogen Energy, 2018, 43(10): 4804–4817
46. Xu P T, McCool N S, Mallouk T E. Water splitting dye-sensitized solar cells. Nano Today, 2017, 14: 42–58
47. Huang Y T, Kavanagh S R, Scanlon D O, Walsh A, Hoye R L Z. Perovskite-inspired materials for photovoltaics and beyond-from design to devices. Nanotechnology, 2021, 32(13): 132004
48. Wang Q, Domen K. Particulate photocatalysts for light-driven water splitting: mechanisms, challenges, and design strategies. Chemical Reviews, 2020, 120(2): 919–985
49. Laskowski F A L, Nellist M R, Qu J J, Boettcher S W. Metal oxide/(oxy)hydroxide overlayers as hole collectors and oxygen-evolution catalysts on water-splitting photoanodes. Journal of the American Chemical Society, 2019, 141(4): 1394–1405
50. Mazzeo A, Santalla S, Gaviglio C, Doctorovich F, Pellegrino J. Recent progress in homogeneous light-driven hydrogen evolution using first-row transition metal catalysts. Inorganica Chimica Acta, 2021, 517: 119950
51. Xu Y, Schoonen M A A. The absolute energy positions of conduction and valence bands of selected semiconducting minerals. American Mineralogist, 2000, 85(3-4): 543–556

52. Bolton J R, Strickler S J, Connolly J S. Limiting and realizable efficiencies of solar photolysis of water. Nature, 1985, 316(6028): 495–500
53. Swathi S, Yuvakkumar R, Ravi G, Babu E S, Velauthapillai D, Alharbi S A. Morphological exploration of chemical vapor-deposited P-doped ZnO nanorods for efficient photoelectrochemical water splitting. Ceramics International, 2021, 47(5): 6521–6527
54. Eidsvag H, Bentouba S, Vajeeston P, Yohi S, Velauthapillai D. TiO_2 as a photocatalyst for water splitting—an experimental and theoretical review. Molecules (Basel, Switzerland), 2021, 26(6): 1687
55. Brillet J, Cornuz M, Formal F L, Yum J H, Grätzel M, Sivula K. Examining architectures of photoanode-photovoltaic tandem cells for solar water splitting. Journal of Materials Research, 2010, 25(1): 17–24
56. Chen Y B, Feng X Y, Liu Y, Guan X J, Burda C, Guo L J. Metal oxide-based tandem cells for self-biased photoelectrochemical water splitting. ACS Energy Letters, 2020, 5(3): 844–866
57. Solarska R, Alexander B D, Augustynski J. Electrochromic and structural characteristics of mesoporous WO_3 films prepared by a sol-gel method. Journal of Solid State Electrochemistry, 2004, 8(10): 748–756
58. Peter L M, Upul Wijayantha K G. Photoelectrochemical water splitting at semiconductor electrodes: fundamental problems and new perspectives. ChemPhysChem, 2014, 15(10): 1983–1995
59. Wu H, Tan H L, Toe C Y, Scott J, Wang L Z, Amal R, Ng Y H. Photocatalytic and photoelectrochemical systems: similarities and differences. Advanced Materials, 2020, 32(18): 1904717
60. Zheng Z X, Lo I M C. Multifunctional photoelectrochemical systems for coupled water treatment and high-value product generation: current status, mechanisms, remaining challenges, and future opportunities. Current Opinion in Chemical Engineering, 2021, 34: 100711
61. Zhou S Q, Chen K Y, Huang J W, Wang L, Zhang M Y, Bai B, Liu H, Wang Q Z. Preparation of heterometallic CoNi-MOFs-modified $BiVO_4$: a steady photoanode for improved performance in photoelectrochemical water splitting. Applied Catalysis B, 2020, 266: 118513
62. Ahmed M, Dincer I. A review on photoelectrochemical hydrogen production systems: challenges and future directions. International Journal of Hydrogen Energy, 2019, 44(5): 2474–2507
63. Bak T, Nowotny J, Rekas M, Sorrell C C. Photo-electrochemical hydrogen generation from water using solar energy, materials-related aspects. International Journal of Hydrogen Energy, 2002, 27(10): 991–1022
64. Vanpoucke D E P, Bultinck P, Cottenier S, Van Speybroeck V, Van Driessche I. Aliovalent doping of CeO_2: DFT study of oxidation state and vacancy effects. Journal of Materials Chemistry A, 2014, 2(33): 13723–13737
65. Liu G, Zhao Y N, Sun C H, Li F, Lu G Q, Cheng H M. Synergistic effects of B/N doping on the visible-light photocatalytic activity of mesoporous TiO_2. Angewandte Chemie International Edition, 2008, 47(24): 4516–4520
66. Long R, English N J. First-principles calculation of synergistic (N, P)-codoping effects on the visible-light photocatalytic activity of anatase TiO_2. Journal of Physical Chemistry C, 2010, 114(27): 11984–11990
67. Niu M, Cheng D J, Cao D P. Enhanced photoelectrochemical performance of anatase TiO_2 by metal-assisted S–O coupling for water splitting. International Journal of Hydrogen Energy, 2013, 38(3): 1251–1257
68. Hu Y F, Huang H T, Feng J Y, Wang W, Guan H M, Li Z S, Zou Z G. Material design and surface/interface engineering of photoelectrodes for solar water splitting. Solar RRL, 2021, 5(4): 2100100
69. Jiao Y, Hellman A, Fang Y R, Gao S W, Kall M. Schottky barrier formation and band bending revealed by first-principles calculations. Scientific Reports, 2015, 5(1): 11374
70. Kwon S, Lee S J, Kim S M, Lee Y, Song H, Park J Y. Probing the nanoscale Schottky barrier of metal/semiconductor interfaces of Pt/CdSe/Pt nanodumbbells by conductive-probe atomic force microscopy. Nanoscale, 2015, 7(29): 12297–12301
71. Tung R T. The physics and chemistry of the Schottky barrier height. Applied Physics Reviews, 2014, 1(1): 011304
72. Zawadzki P, Laursen A B, Jacobsen K W, Dahl S, Rossmeisl J. Oxidative trends of TiO_2-hole trapping at anatase and rutile surfaces. Energy & Environmental Science, 2012, 5(12): 9866–9869
73. Alexandrov V, Neumann A, Scherer M M, Rosso K M. Electron exchange and conduction in nontronite from first-principles. Journal of Physical Chemistry C, 2013, 117(5): 2032–2040
74. Jafari T, Moharreri E, Amin A S, Miao R, Song W, Suib S L. Photocatalytic water splitting-the untamed dream: a review of recent advances. Molecules (Basel, Switzerland), 2016, 21(7): 900
75. Zou Z, Ye J, Sayama K, Arakawa H. Direct splitting of water under visible light irradiation with an oxide semiconductor photocatalyst. Nature, 2001, 414(6864): 625–627
76. Riss A, Elser M J, Bernardi J, Diwald O. Stability and photoelectronic properties of layered titanate nanostructures. Journal of the American Chemical Society, 2009, 131(17): 6198–6206
77. Wickman B, Bastos Fanta A, Burrows A, Hellman A, Wagner J B, Iandolo B. Iron oxide films prepared by rapid thermal processing for solar energy conversion. Scientific Reports, 2017, 7(1): 40500
78. Xia Y, Yang P, Sun Y, Wu Y, Mayers B, Gates B, Yin Y, Kim F, Yan H. One-dimensional nanostructures: synthesis, characterization, and applications. Advanced Materials, 2003, 15(5): 353–389
79. Mahalingam S, Abdullah H. Electron transport study of indium oxide as photoanode in DSSCs: a review. Renewable & Sustainable Energy Reviews, 2016, 63: 245–255
80. Xu J, Wang Z, Li W, Zhang X, He D, Xiao X. Ag nanoparticles located on three-dimensional pine tree-like hierarchical TiO_2 nanotube array films as high-efficiency plasmonic photocatalysts. Nanoscale Research Letters, 2017, 12(1): 54
81. Bedin K C, Muche D N F, Melo M A Jr, Freitas A L M, Gonçalves R V, Souza F L. Role of cocatalysts on hematite photoanodes in photoelectrocatalytic water splitting: challenges

and future perspectives. ChemCatChem, 2020, 12(12): 3156–3169

82. Rajaambal S, Sivaranjani K, Gopinath C S. Recent developments in solar H_2 generation from water splitting. Journal of Chemical Sciences, 2015, 127(1): 33–47
83. Zafar Z, Yi S S, Li J P, Li C Q, Zhu Y F, Zada A, Yao W J, Liu Z Y, Yue X Z. Recent development in defects engineered photocatalysts: an overview of the experimental and theoretical strategies. Energy & Environmental Materials, 2021. doi: 10.1002/eem1002.12171
84. Zhang P, Lou X W. Design of heterostructured hollow photocatalysts for solar-to-chemical energy conversion. Advanced Materials, 2019, 31(29): 1900281
85. Chen S R, Li C L, Hou Z Y. The novel behavior of photoelectrochemical property of annealing TiO_2 nanorod arrays. Journal of Materials Science, 2020, 55(14): 5969–5981
86. Joo J B, Zhang Q, Dahl M, Lee I, Goebl J, Zaera F, Yin Y D. Control of the nanoscale crystallinity in mesoporous TiO_2 shells for enhanced photocatalytic activity. Energy & Environmental Science, 2012, 5(4): 6321–6327
87. Tan H L, Amal R, Ng Y H. Alternative strategies in improving the photocatalytic and photoelectrochemical activities of visible light-driven $BiVO_4$: a review. Journal of Materials Chemistry. A, Materials for Energy and Sustainability, 2017, 5(32): 16498–16521
88. Yan Z Y, Huang W X, Jiang X R, Gao J Z, Hu Y W, Zhang H Z, Shi Q W. Hollow structured black TiO_2 with thickness-controllable microporous shells for enhanced visible-light-driven photocatalysis. Microporous and Mesoporous Materials, 2021, 323: 111228
89. Zhang W, Tian Y, He H L, Xu L, Li W, Zhao D Y. Recent advances in the synthesis of hierarchically mesoporous TiO_2 materials for energy and environmental applications. National Science Review, 2020, 7(11): 1702–1725
90. Pihosh Y, Minegishi T, Nandal V, Higashi T, Katayama M, Yamada T, Sasaki Y, Seki K, Suzuki Y, Nakabayashi M, et al. Ta_3N_5-nanorods enabling highly efficient water oxidation via advantageous light harvesting and charge collection. Energy & Environmental Science, 2020, 13(5): 1519–1530
91. Cao M Q, Li H M, Liu K, Hu J H, Pan H, Fu J W, Liu M. Vertical $SrNbO_2N$ nanorod arrays for solar-driven photoelectrochemical water splitting. Solar RRL, 2021, 5(6): 2000448
92. Chen X B, Liu L, Yu P Y, Mao S S. Increasing solar absorption for photocatalysis with black hydrogenated titanium dioxide nanocrystals. Science, 2011, 331(6018): 746–750
93. Takagi F, Kageshima Y, Teshima K, Domen K, Nishikiori H. Enhanced photoelectrochemical performance from particulate ZnSe:Cu(In,Ga)Se-2 photocathodes during solar hydrogen production via particle size control. Sustainable Energy & Fuels, 2021, 5(2): 412–423
94. Mishra A K, Pradhan D. Morphology controlled solution-based synthesis of Cu_2O crystals for the facets-dependent catalytic reduction of highly toxic aqueous Cr(VI). Crystal Growth & Design, 2016, 16(7): 3688–3698
95. Tan H L, Amal R, Ng Y H. Exploring the different roles of particle size in photoelectrochemical and photocatalytic water oxidation on $BiVO_4$. ACS Applied Materials & Interfaces, 2016, 8(42): 28607–28614
96. Xiao M, Wang Z L, Lyu M Q, Luo B, Wang S C, Liu G, Cheng H M, Wang L Z. Hollow nanostructures for photocatalysis: advantages and challenges. Advanced Materials, 2019, 31(38): 1801369
97. Kim K, Moon J H. Three-dimensional bicontinuous $BiVO_4$/ZnO photoanodes for high solar water-splitting performance at low bias potential. ACS Applied Materials & Interfaces, 2018, 10(40): 34238–34244
98. Osterloh F E. Inorganic nanostructures for photoelectrochemical and photocatalytic water splitting. Chemical Society Reviews, 2013, 42(6): 2294–2320
99. Reddy N L, Emin S, Valant M, Shankar M V. Nanostructured Bi_2O_3@TiO_2 photocatalyst for enhanced hydrogen production. International Journal of Hydrogen Energy, 2017, 42(10): 6627–6636
100. Yin J, Liao G Z, Zhou J L, Huang C M, Ling Y, Lu P, Li L S. High performance of magnetic $BiFeO_3$ nanoparticle-mediated photocatalytic ozonation for wastewater decontamination. Separation and Purification Technology, 2016, 168: 134–140
101. Eftekhari A, Babu V J, Ramakrishna S. Photoelectrode nanomaterials for photoelectrochemical water splitting. International Journal of Hydrogen Energy, 2017, 42(16): 11078–11109
102. Vishwakarma A K, Tripathi P, Srivastava A, Sinha A S K, Srivastava O N. Band gap engineering of Gd and Co doped $BiFeO_3$ and their application in hydrogen production through photoelectrochemical route. International Journal of Hydrogen Energy, 2017, 42(36): 22677–22686
103. Wang J J, Sun H F, Huang J, Li Q X, Yang J L. Band structure tuning of TiO_2 for enhanced photoelectrochemical water splitting. Journal of Physical Chemistry C, 2014, 118(14): 7451–7457
104. Momeni M M, Akbarnia M, Ghayeb Y. Preparation of S-W-codoped TiO_2 nanotubes and effect of various hole scavengers on their photoelectrochemical activity: alcohol series. International Journal of Hydrogen Energy, 2020, 45(58): 33552–33562
105. Ghosh D, Roy K, Sarkar K, Devi P, Kumar P. Surface plasmon-enhanced carbon dot-embellished multifaceted Si(111) nanoheterostructure for photoelectrochemical water splitting. ACS Applied Materials & Interfaces, 2020, 12(25): 28792–28800
106. Kumar D, Sharma S, Khare N. Enhanced photoelectrochemical performance of plasmonic Ag nanoparticles grafted ternary Ag/PaNi/$NaNbO_3$ nanocomposite photoanode for photoelectrochemical water splitting. Renewable Energy, 2020, 156: 173–182
107. Li H X, Li X, Dong W, Xi J H, Du G, Ji Z G. Cu nanoparticles hybridized with ZnO thin film for enhanced photoelectrochemical oxygen evolution. Journal of Alloys and Compounds, 2018, 768: 830–837
108. Li Z, Shi L, Franklin D, Koul S, Kushima A, Yang Y. Drastic enhancement of photoelectrochemical water splitting performance over plasmonic Al@TiO_2 heterostructured nanocavity arrays. Nano Energy, 2018, 51: 400–407

109. Zheng Z K, Xie W, Huang B B, Dai Y. Plasmon-enhanced solar water splitting on metal-semiconductor photocatalysts. Chemistry (Weinheim an der Bergstrasse, Germany), 2018, 24(69): 18322–18333
110. Warren S C, Thimsen E. Plasmonic solar water splitting. Energy & Environmental Science, 2012, 5(1): 5133–5146
111. Lee J, Mubeen S, Ji X, Stucky G D, Moskovits M. Plasmonic photoanodes for solar water splitting with visible light. Nano Letters, 2012, 12(9): 5014–5019
112. Onishi T, Teranishi M, Naya S, Fujishima M, Tada H. Electrocatalytic effect on the photon-to-current conversion efficiency of gold-nanoparticle-loaded titanium(IV) oxide plasmonic electrodes for water oxidation. Journal of Physical Chemistry C, 2020, 124(11): 6103–6109
113. Patra B K, Khilari S, Pradhan D, Pradhan N. Hybrid dot-disk Au-$CuInS_2$ nanostructures as active photocathode for efficient evolution of hydrogen from water. Chemistry of Materials, 2016, 28(12): 4358–4366
114. Lickleder M, Mohammadi R, Nguyen N T, Park H, Hejazi S, Halik M, Vogel N, Altomare M, Schmuki P. Dewetted Au nanoparticles on TiO_2 surfaces: evidence of a size-independent plasmonic photoelectrochemical response. Journal of Physical Chemistry C, 2019, 123(27): 16934–16942
115. Dutta A, Pihuleac B, Chen Y, Zong C, Dal Negro L, Yang C. Au@SiO_2@Au core-shell-shell nanoparticles for enhancing photocatalytic activity of hematite. Materials Today Energy, 2021, 19: 100576
116. Haider R S, Wang S, Gao Y, Malik A S, Ta N, Li H, Zeng B, Dupuis M, Fan F, Li C. Boosting photocatalytic water oxidation by surface plasmon resonance of Ag_xAu_{1-x} alloy nanoparticles. Nano Energy, 2021, 87: 106189
117. Haydous F, Luo S J, Wu K T, Lawley C, Dobeli M, Ishihara T, Lippert T. Surface analysis of perovskite oxynitride thin films as photoelectrodes for solar water splitting. ACS Applied Materials & Interfaces, 2021, 13(31): 37785–37796
118. Higashi M, Domen K, Abe R. Fabrication of efficient TaON and Ta_3N_5 photoanodes for water splitting under visible light irradiation. Energy & Environmental Science, 2011, 4(10): 4138–4147
119. Bae D, Seger B, Vesborg P C K, Hansen O, Chorkendorff I. Strategies for stable water splitting via protected photoelectrodes. Chemical Society Reviews, 2017, 46(7): 1933–1954
120. Ros C, Carretero N M, David J, Arbiol J, Andreu T, Morante J R. Insight into the degradation mechanisms of atomic layer deposited TiO_2 as photoanode protective layer. ACS Applied Materials & Interfaces, 2019, 11(33): 29725–29735
121. Wang R, Wang L, Zhou Y, Zou Z. Al-ZnO/CdS photoanode modified with a triple functions conformal TiO_2 film for enhanced photoelectrochemical efficiency and stability. Applied Catalysis B, 2019, 255: 117738
122. Hu S, Lewis N S, Ager J W, Yang J, McKone J R, Strandwitz N C. Thin-film materials for the protection of semiconducting photoelectrodes in solar-fuel generators. Journal of Physical Chemistry C, 2015, 119(43): 24201–24228
123. Kenney M J, Gong M, Li Y G, Wu J Z, Feng J, Lanza M, Dai H J. High-performance silicon photoanodes passivated with ultrathin nickel films for water oxidation. Science, 2013, 342(6160): 836–840
124. Ros C, Andreu T, David J, Arbiol J, Morante J R. Degradation and regeneration mechanisms of NiO protective layers deposited by ALD on photoanodes. Journal of Materials Chemistry. A, Materials for Energy and Sustainability, 2019, 7(38): 21892–21902
125. McDowell M T, Lichterman M F, Spurgeon J M, Hu S, Sharp I D, Brunschwig B S, Lewis N S. Improved stability of polycrystalline bismuth vanadate photoanodes by use of dual-layer thin TiO_2/Ni coatings. Journal of Physical Chemistry C, 2014, 118(34): 19618–19624
126. Fan R L, Dong W, Fang L, Zheng F G, Su X D, Zou S, Huang J, Wang X S, Shen M R. Stable and efficient multi-crystalline n + p silicon photocathode for H_2 production with pyramid-like surface nanostructure and thin Al_2O_3 protective layer. Applied Physics Letters, 2015, 106(1): 013902
127. Pavlenko M, Siuzdak K, Coy E, Załęski K, Jancelewicz M, Iatsunskyi I. Enhanced solar-driven water splitting of 1D core-shell Si/TiO_2/ZnO nanopillars. International Journal of Hydrogen Energy, 2020, 45(50): 26426–26433
128. Ashcheulov P, Taylor A, Mortet V, Poruba A, Le Formal F, Krýsová H, Klementová M, Hubík P, Kopeček J, Lorinčík J, et al. Nanocrystalline boron-doped diamond as a corrosion-resistant anode for water oxidation via Si photoelectrodes. ACS Applied Materials & Interfaces, 2018, 10(35): 29552–29564
129. Coy E, Siuzdak K, Grądzka-Kurzaj I, Sayegh S, Weber M, Ziółek M, Bechelany M, Iatsunskyi I. Exploring the effect of BN and B-N bridges on the photocatalytic performance of semiconductor heterojunctions: enhancing carrier transfer mechanism. Applied Materials Today, 2021, 24: 101095
130. Yang W, Prabhakar R R, Tan J, Tilley S D, Moon J. Strategies for enhancing the photocurrent, photovoltage, and stability of photoelectrodes for photoelectrochemical water splitting. Chemical Society Reviews, 2019, 48(19): 4979–5015
131. Zhao X, Luo W J, Feng J Y, Li M X, Li Z S, Yu T, Zou Z G. Quantitative analysis and visualized evidence for high charge separation efficiency in a solid-liquid bulk heterojunction. Advanced Energy Materials, 2014, 4(9): 1301785
132. Safa S, Khajeh M, Oveisi A R, Azimirad R, Salehzadeh H. Photocatalytic performance of graphene quantum dot incorporated UiO-66-NH_2 composite assembled on plasma-treated membrane. Advanced Powder Technology, 2021, 32(4): 1081–1087
133. Sang L X, Lin J, Zhao Y B. Preparation of carbon dots/TiO_2 electrodes and their photoelectrochemical activities for water splitting. International Journal of Hydrogen Energy, 2017, 42(17): 12122–12132
134. Wang P, Zhou X B, Shao Y, Li D Z, Zuo Z F, Liu X Z. CdS quantum dots-decorated InOOH: facile synthesis and excellent photocatalytic activity under visible light. Journal of Colloid and Interface Science, 2021, 601: 186–195
135. Wen P, Li H, Ma X, Lei R B, Wang X W, Geyer S M, Qiu Y J. A colloidal ZnTe quantum dot-based photocathode with a metal-insulator-semiconductor structure towards solar-driven CO_2

reduction to tunable syngas. Journal of Materials Chemistry A, 2021, 9(6): 3589–3596

136. Zhu C, Liu C G, Zhou Y J, Fu Y J, Guo S J, Li H, Zhao S Q, Huang H, Liu Y, Kang Z H. Carbon dots enhance the stability of CdS for visible-light-driven overall water splitting. Applied Catalysis B, 2017, 216: 114–121
137. Deshmukh P R, Sohn Y, Shin W G. Chemical synthesis of ZnO nanorods: investigations of electrochemical performance and photo-electrochemical water splitting applications. Journal of Alloys and Compounds, 2017, 711: 573–580
138. Mohajernia S, Hejazi S, Mazare A, Nguyen N T, Schmuki P. Photoelectrochemical H_2 generation from suboxide TiO_2 nanotubes: visible-light absorption versus conductivity. Chemistry (Weinheim an der Bergstrasse, Germany), 2017, 23(50): 12406–12411
139. Tiwari J N, Singh A N, Sultan S, Kim K S. Recent advancement of *p*- and *d*-block elements, single atoms, and graphene-based photoelectrochemical electrodes for water splitting. Advanced Energy Materials, 2020, 10(24): 2000280
140. Cosham S D, Celorrio V, Kulak A N, Hyett G. Observation of visible light activated photocatalytic degradation of stearic acid on thin films of tantalum oxynitride synthesized by aerosol assisted chemical vapour deposition. Dalton Transactions (Cambridge, England), 2019, 48(28): 10619–10627
141. Iborra-Torres A, Kulak A N, Palgrave R G, Hyett G. Demonstration of visible light-activated photocatalytic self-cleaning by thin films of perovskite tantalum and niobium oxynitrides. ACS Applied Materials & Interfaces, 2020, 12(30): 33603–33612
142. Mami A, Saafi I, Larbi T, Ben Messaoud K, Yacoubi N, Amlouk M. Unraveling the effect of thickness on the structural, morphological, opto-thermal and DFT calculation of hematite Fe_2O_3 thin films for photo-catalytic application. Journal of Materials Science Materials in Electronics, 2021, 32(13): 17974–17989
143. Hou Y, Zuo F, Dagg A, Feng P Y. A three-dimensional branched cobalt-doped alpha-Fe_2O_3 nanorod/$MgFe_2O_4$ heterojunction array as a flexible photoanode for efficient photoelectrochemical water oxidation. Angewandte Chemie International Edition, 2013, 52(4): 1248–1252
144. Hou Y, Zuo F, Dagg A P, Liu J K, Feng P Y. Branched WO_3 nanosheet array with layered C_3N_4 heterojunctions and CoO_x nanoparticles as a flexible photoanode for efficient photoelectrochemical water oxidation. Advanced Materials, 2014, 26(29): 5043–5049
145. Zhang X, Liu Y, Kang Z H. 3D branched ZnO nanowire arrays decorated with plasmonic Au manoparticles for high-performance photoelectrochemical water splitting. ACS Applied Materials & Interfaces, 2014, 6(6): 4480–4489
146. Zhang C X, Zhao P Y, Liu S X, Yu K. Three-dimensionally ordered macroporous perovskite materials for environmental applications. Chinese Journal of Catalysis, 2019, 40(9): 1324–1338
147. Cho I S, Chen Z B, Forman A J, Kim D R, Rao P M, Jaramillo T F, Zheng X L. Branched TiO_2 nanorods for photoelectrochemical hydrogen production. Nano Letters, 2011, 11(11): 4978–4984
148. Warren S C, Voitchovsky K, Dotan H, Leroy C M, Cornuz M, Stellacci F, Hebert C, Rothschild A, Gratzel M. Identifying champion nanostructures for solar water-splitting. Nature Materials, 2013, 12(9): 842–849
149. Chen S, Huang D L, Xu P A, Xue W J, Lei L, Cheng M, Wang R Z, Liu X G, Deng R. Semiconductor-based photocatalysts for photocatalytic and photoelectrochemical water splitting: will we stop with photocorrosion? Journal of Materials Chemistry A, 2020, 8(5): 2286–2322
150. Wolcott A, Smith W A, Kuykendall T R, Zhao Y P, Zhang J Z. Photoelectrochemical water splitting using dense and aligned TiO_2 nanorod arrays. Small, 2009, 5(1): 104–111
151. Viter R, Iatsunskyi I, Fedorenko V, Tumenas S, Balevicius Z, Ramanavicius A, Balme S, Kempiński M, Nowaczyk G, Jurga S, et al. Enhancement of electronic and optical properties of ZnO/Al_2O_3 nanolaminate coated electrospun nanofibers. Journal of Physical Chemistry C, 2016, 120(9): 5124–5132
152. Iatsunskyi I, Coy E, Viter R, Nowaczyk G, Jancelewicz M, Baleviciute I, Zaleski K, Jurga S. Study on structural, mechanical, and optical properties of Al_2O_3-TiO_2 nanolaminates prepared by atomic layer deposition. Journal of Physical Chemistry C, 2015, 119(35): 20591–20599
153. Wen P, Sun Y H, Li H, Liang Z Q, Wu H H, Zhang J C, Zeng H J, Geyer S M, Jiang L. A highly active three-dimensional Z-scheme ZnO/Au/g-C_3N_4 photocathode for efficient photoelectrochemical water splitting. Applied Catalysis B, 2020, 263: 118180
154. Maeda K, Higashi M, Lu D L, Abe R, Domen K. Efficient nonsacrificial water splitting through two-step photoexcitation by visible light using a modified oxynitride as a hydrogen evolution photocatalyst. Journal of the American Chemical Society, 2010, 132(16): 5858–5868
155. Wang X W, Liu G, Chen Z G, Li F, Wang L Z, Lu G Q, Cheng H M. Enhanced photocatalytic hydrogen evolution by prolonging the lifetime of carriers in ZnO/CdS heterostructures. Chemical Communications, 2009(23): 3452–3454
156. Kato H, Sasaki Y, Iwase A, Kudo A. Role of iron ion electron mediator on photocatalytic overall water splitting under visible light irradiation using Z-scheme systems. Bulletin of the Chemical Society of Japan, 2007, 80(12): 2457–2464
157. Chen S S, Vequizo J J M, Pan Z H, Hisatomi T, Nakabayashi M, Lin L H, Wang Z, Kato K, Yamakata A, Shibata N, et al. Surface modifications of $(ZnSe)_{0.5}(CuGa_{2.5}Se_{4.25})_{0.5}$ to promote photocatalytic Z-scheme overall water splitting. Journal of the American Chemical Society, 2021, 143(28): 10633–10641
158. Ng B J, Putri L K, Kong X Y, Pasbakhsh P, Chai S P. Z-scheme photocatalyst sheets with P-doped twinned $Zn_{0.5}Cd_{0.5}S_{1-x}$ and Bi_4NbO_8Cl connected by carbon electron mediator for overall water splitting under ambient condition. Chemical Engineering Journal, 2021, 404: 127030
159. Wang Z L, Chen Z, Dan J D, Chen W Q, Zhou C H, Shen Z X, Sum Z C, Wang X S. Improving photoelectrochemical activity of ZnO/TiO_2 core-shell nanostructure through Ag nanoparticle integration. Catalysts, 2021, 11(8): 911
160. Lyu S, Farre Y, Ducasse L, Pellegrin Y, Toupance T, Olivier C,

Odobel F. Push-pull ruthenium diacetylide complexes: new dyes for p-type dye-sensitized solar cells. RSC Advances, 2016, 6(24): 19928–19936

161. Lyu S, Massin J, Pavone M, Munoz-Garcia A B, Labrugere C, Toupance T, Chavarot-Kerlidou M, Artero V, Olivier C. H_2-evolving dye-sensitized photocathode based on a ruthenium-diacetylide/cobaloxime supramolecular assembly. ACS Applied Energy Materials, 2019, 2(7): 4971–4980
162. Massin J, Lyu S, Pavone M, Munoz-Garcia A B, Kauffmann B, Toupance T, Chavarot-Kerlidou M, Artero V, Olivier C. Design and synthesis of novel organometallic dyes for NiO sensitization and photo-electrochemical applications. Dalton Transactions (Cambridge, England), 2016, 45(31): 12539–12547
163. Brillet J, Yum J H, Cornuz M, Hisatomi T, Solarska R, Augustynski J, Graetzel M, Sivula K. Highly efficient water splitting by a dual-absorber tandem cell. Nature Photonics, 2012, 6(12): 823–827
164. Kim J K, Shin K, Cho S M, Lee T W, Park J H. Synthesis of transparent mesoporous tungsten trioxide films with enhanced photoelectrochemical response: application to unassisted solar water splitting. Energy & Environmental Science, 2011, 4(4): 1465–1470
165. Fu X C, Chang H, Shang Z C, Liu P L, Liu J K, Luo H A. Three-dimensional Cu_2O nanorods modified by hydrogen treated $Ti_3C_2T_x$ MXene with enriched oxygen vacancies as a photocathode and a tandem cell for unassisted solar water splitting. Chemical Engineering Journal, 2020, 381: 122001
166. Peerakiatkhajohn P, Yun J H, Wang S C, Wang L Z. Review of recent progress in unassisted photoelectrochemical water splitting: from material modification to configuration design. Journal of Photonics for Energy, 2017, 7(1): 012006
167. Kim J H, Jo Y, Kim J H, Jang J W, Kang H J, Lee Y H, Kim D S, Jun Y, Lee J S. Wireless solar water splitting device with robust cobalt-catalyzed, dual-doped $BiVO_4$ photoanode and perovskite solar cell in tandem: a dual absorber artificial leaf. ACS Nano, 2015, 9(12): 11820–11829
168. Luo J S, Im J H, Mayer M T, Schreier M, Nazeeruddin M K, Park N G, Tilley S D, Fan H J, Gratzel M. Water photolysis at 12.3% efficiency via perovskite photovoltaics and Earth-abundant catalysts. Science, 2014, 345(6204): 1593–1596
169. Wang S C, Chen P, Bai Y, Yun J H, Liu G, Wang L Z. New $BiVO_4$ dual photoanodes with enriched oxygen vacancies for efficient solar-driven water splitting. Advanced Materials, 2018, 30(20): 1800486
170. Bera S, Lee S A, Lee W J, Kim J H, Kim C, Kim H G, Khan H, Jana S, Jang H W, Kwon S H. Hierarchical nanoporous $BiVO_4$ photoanodes with high charge separation and transport efficiency for water oxidation. ACS Applied Materials & Interfaces, 2021, 13(12): 14304–14314
171. Mor G K, Varghese O K, Wilke R H T, Sharma S, Shankar K, Latempa T J, Choi K S, Grimes C A. p-Type Cu–Ti–O nanotube arrays and their use in self-biased heterojunction photoelectrochemical diodes for hydrogen generation. Nano Letters, 2008, 8(7): 1906–1911
172. Oh S, Song H, Oh J. An optically and electrochemically decoupled monolithic photoelectrochemical cell for high-performance solar-driven water splitting. Nano Letters, 2017, 17(9): 5416–5422
173. Ganesh V, Alizadeh M, Shuhaimi A, Adreen A, Pandikumar A, Jayakumar M, Huang N M, Ramesh R, Baskar K, Rahman S A. Correlation between indium content in monolithic InGaN/GaN multi quantum well structures on photoelectrochemical activity for water splitting. Journal of Alloys and Compounds, 2017, 706: 629–636
174. Zhu J J, Gudmundsdottir J B, Strandbakke R, Both K G, Aarholt T, Carvalho P A, Sorby M H, Jensen I J T, Guzik M N, Norby T, Haug H, Chatzitakis A. Double perovskite cobaltites integrated in a monolithic and noble metal-free photoelectrochemical device for efficient water splitting. ACS Applied Materials & Interfaces, 2021, 13(17): 20313–20325
175. Ahmet I Y, Berglund S, Chemseddine A, Bogdanoff P, Präg R F, Abdi F F, van de Krol R. Planar and nanostructured *n*-Si/metal-oxide/WO_3/$BiVO_4$ monolithic tandem devices for unassisted solar water splitting. Advanced Energy and Sustainability Research, 2020, 1(2): 2000037
176. Vanka S, Zhou B W, Awni R A, Song Z N, Chowdhury F A, Liu X D, Hajibabaei H, Shi W, Xiao Y X, Navid I A, et al. InGaN/Si double-junction photocathode for unassisted solar water splitting. ACS Energy Letters, 2020, 5(12): 3741–3751